



# Building thermal modeling and model predictive control with physically consistent deep learning for decarbonization and energy optimization

Tianqi Xiao<sup>a</sup>, Fengqi You<sup>a,b,\*</sup>

<sup>a</sup> Systems Engineering, Cornell University, Ithaca, NY 14853, USA

<sup>b</sup> Robert Frederick Smith School of Chemical and Biomolecular Engineering, Cornell University, Ithaca, NY 14853, USA

## HIGHLIGHT

- A novel physically consistent deep learning framework for building thermal modeling.
- A PCDL-based MPC for optimizing energy efficiency and indoor thermal comfort.
- A simulation case study of an office building at Cornell University.

## ARTICLE INFO

### Keywords:

Deep Learning  
Physics Consistency  
Model Predictive Control  
Building Energy Efficiency Optimization  
Decarbonization

## ABSTRACT

Being a primary contributor to global energy consumption and energy-related carbon emissions, the building and building construction sectors are a crucial player in the decarbonization and energy efficiency efforts. This article proposes a novel physically consistent deep learning (PCDL) approach for building thermal modeling and assesses its potential for optimizing building energy efficiency and indoor thermal comfort through model predictive control (MPC). The PCDL model considers physical relationships between system inputs and outputs and is applied to predict the indoor thermal climate. With the strict guarantee of satisfying the laws of physics, the proposed PCDL model has better generalization ability than other machine learning approaches. Subsequently, the PCDL model is integrated into an MPC controller to optimize building energy consumption and indoor thermal comfort. The proposed approach is tested on Carpenter Hall, a multi-zone office building located in Cornell University Campus, through simulations. Based on the simulation results, the PCDL model demonstrate a much better generalization ability for yielding physically-feasible predictions compared to the long short-term memory (LSTM) model. Compared to an On/Off controller, a state space model-based MPC controller, and an LSTM-based MPC controller, the proposed PCDL-based MPC reduces by 5.8%, 4.5%, and 8.9% energy consumption and improves by 55%, 59%, and 64% indoor thermal comfort, respectively, and therefore enhances the building decarbonization progress. The results emphasize the importance of considering physics information in data-driven models and highlight the advantages of the proposed PCDL-based MPC controller.

## 1. Introduction

Smart buildings use advanced computing and artificial intelligence (AI) technologies to improve energy efficiency, promote decarbonization, and enhance user experiences. According to the International Energy Agency's report from 2022, the building and building construction sectors account for 30% of global energy consumption and 27% of global energy-related emissions [1]. Conventional buildings struggle to meet energy efficiency and decarbonization goals due to limited sensors and computing sources [2]. However, smart buildings

can alleviate this problem by incorporating the Internet of Things (IoT) with AI in building energy management (BEM) systems [3]. These systems collect data from sensors and devices, analyze it using AI methods, and apply the insights to optimize energy consumption and reduce carbon emissions while meeting residents' needs [4,5]. The applications of AI methods in BEM systems vary and can be categorized as occupant-oriented (e.g., pattern recognition and behavior estimation) and device-oriented (e.g., load prediction and fault detection) [6]. These AI-based approaches enable buildings to be sustainable and energy efficient by augmenting the ability of the control systems to cope with complex dynamics and behaviors.

\* Corresponding author at: Systems Engineering, Cornell University, Ithaca, NY 14853, USA.

E-mail address: [fengqi.you@cornell.edu](mailto:fengqi.you@cornell.edu) (F. You).

<b>Nomenclature</b>	
<i>Abbreviations</i>	
<i>AI</i>	Artificial Intelligence
<i>BEM</i>	Building energy management
<i>BRCM</i>	Building resistance–capacitance model
<i>GPU</i>	Graphics processing unit
<i>HVAC</i>	Heating, ventilation, and air conditioning
<i>IoT</i>	Internet of Things
<i>LSTM</i>	Long short-term memory
<i>MAE</i>	Mean absolute error
<i>MIMO</i>	Multiple-input multiple-output
<i>MLP</i>	Multilayer perceptron
<i>MPC</i>	Model predictive control
<i>MSE</i>	Mean square error
<i>NN</i>	Neural network
<i>PCDL</i>	Physically consistent deep learning
<i>PCNN</i>	Physically consistent neural network
<i>PDE</i>	Partial differential equation
<i>PID</i>	Proportional–integral–derivative
<i>PiNN</i>	Physics-informed neural network
<i>PMV</i>	Predicted mean vote
<i>RNN</i>	Recurrent neural network
<i>SISO</i>	Single-input single-output
<i>SSM</i>	State space model
<i>Parameters</i>	
<i>A</i>	Area ( $\text{m}^2$ )
<i>A</i>	State matrix (unitless)
<i>B</i>	Input matrix (unitless)
<i>c</i>	Memory state of the LSTM cell (unitless)
<i>Cap</i>	Capacity ( $\text{m}^3$ )
<i>h</i>	Hidden state of the LSTM cell (unitless)
$\tilde{h}$	Hidden state of the RNN cell (unitless)
<i>H</i>	Absolute humidity ( $\text{kg}/\text{m}^3$ )
$\dot{m}$	Mass flow ( $\text{kg}/\text{s}$ )
<i>MR</i>	Metabolic rate ( $\text{W}/\text{m}^2$ )
<i>P</i>	Pressure (kPa)
<i>PMV</i>	Predicted mean vote (unitless)
<i>Q</i>	Thermal Power (W)
<i>R</i>	Ratio (Unitless)
<i>RH</i>	Relative Humidity (%)
<i>T</i>	Temperature ( $^\circ\text{C}$ )
<i>u</i>	Control variables (unitless)
<i>U</i>	Power (kW)
<i>V</i>	Volume ( $\text{m}^3$ )
<i>x</i>	Inputs without physics consistency (unitless)
$\tilde{x}$	Inputs with physics consistency (unitless)
<i>x</i>	System states (unitless)
<i>z</i>	Disturbances (unitless)
<i>Z</i>	Outputs of the PCDL model (unitless)
<i>e</i>	Slack variables (unitless)
<i>ρ</i>	Density ( $\text{kg}/\text{m}^3$ )
<i>Subscripts</i>	
<i>add</i>	Additional rate
<i>air</i>	Air
<i>cool</i>	Cooling
<i>dehum</i>	Dehumidification
<i>diff</i>	Difference
<i>e</i>	Exterior environment
<i>fan</i>	Fan
<i>heat</i>	Heating
<i>hh</i>	Hidden states to hidden states
<i>hum</i>	Humidifier
<i>i</i>	Past timestep
<i>ig</i>	Internal gain
<i>ih</i>	Input to hidden state
<i>in</i>	Inlet
<i>j</i>	Zone number
<i>k</i>	Timestep
<i>LB</i>	Lower bound
<i>mr</i>	Mean radiant
<i>ne</i>	Neighbor zones
<i>nom</i>	Nominal
<i>PCDL</i>	The PCDL model
<i>sat</i>	Saturated
<i>SSM</i>	The state space model
<i>stdy</i>	Standby
<i>surf</i>	Surface
<i>UB</i>	Upper bound
<i>vent</i>	Ventilation system
<i>xu</i>	Inputs to control variables
<i>zu</i>	Disturbances to control variables

As a critical element in the design [7], retrofitting [8], and control [9] of BEM systems, building modeling has been an active area of research for ages. Generally, these models can be divided into three categories: white-box (physics-based) models, black-box (data-based) models, and grey-box (physics-data-hybrid) models. White-box models are based on physics principles like constrained partial differential equations (PDEs). Various physics-based simulation tools, such as EnergyPlus [10], TRNSYS [11], IDA ICE [12], and Modelica [13], have been developed for building modeling. However, these tools require extensive expert intervention and high computational demands for high accuracy [14]. Taking advantage of vast amounts of data with the widespread of IoTs and the recent developments of the graphics processing unit (GPU) and AI algorithms, black-box models, such as machine learning and deep learning models, have been developed and applied for approximating system dynamics accurately without any physics principles in the formation [15,16]. These models have been validated in many application cases [17,18]. However, black-box models are subject to their low generalization ability, lack of safety and interpretability guarantee, and extreme sensitivity to data quality and quantity [19,20]. Grey-box model is a combination of white-box and

black-box models. A typical example of building modeling is the resistance–capacitance (RC) model, in which thermal masses are treated as resistors and capacitors based on physics principles [21,22]. Nevertheless, to make trade-offs between accuracy and complexity, most grey-box models cannot approximate highly nonlinear behaviors in building systems [23]. Furthermore, complex modeling and identification procedures still need specialized interventions [24]. Therefore, a more reliable and accurate control-oriented modeling method is needed for building energy optimization.

To overcome the limitations of existing modeling methods, researchers have explored incorporating prior physics-based knowledge into AI models. Pioneer works include the physics-guided neural network published by Karpatne et al. [25] and the physics-informed neural network (PiNN) developed by Raissi et al. [26] in 2017, with many subsequent articles proposing extended and modified versions based on similar ideas [27,28]. Although physics-informed AI models have been implemented in many fields, their applications in building modeling have yet to be deeply explored [29]. The first work in this area was published in 2021, in which researchers generated a block-based neural network with constraints on its weighting matrix and cost

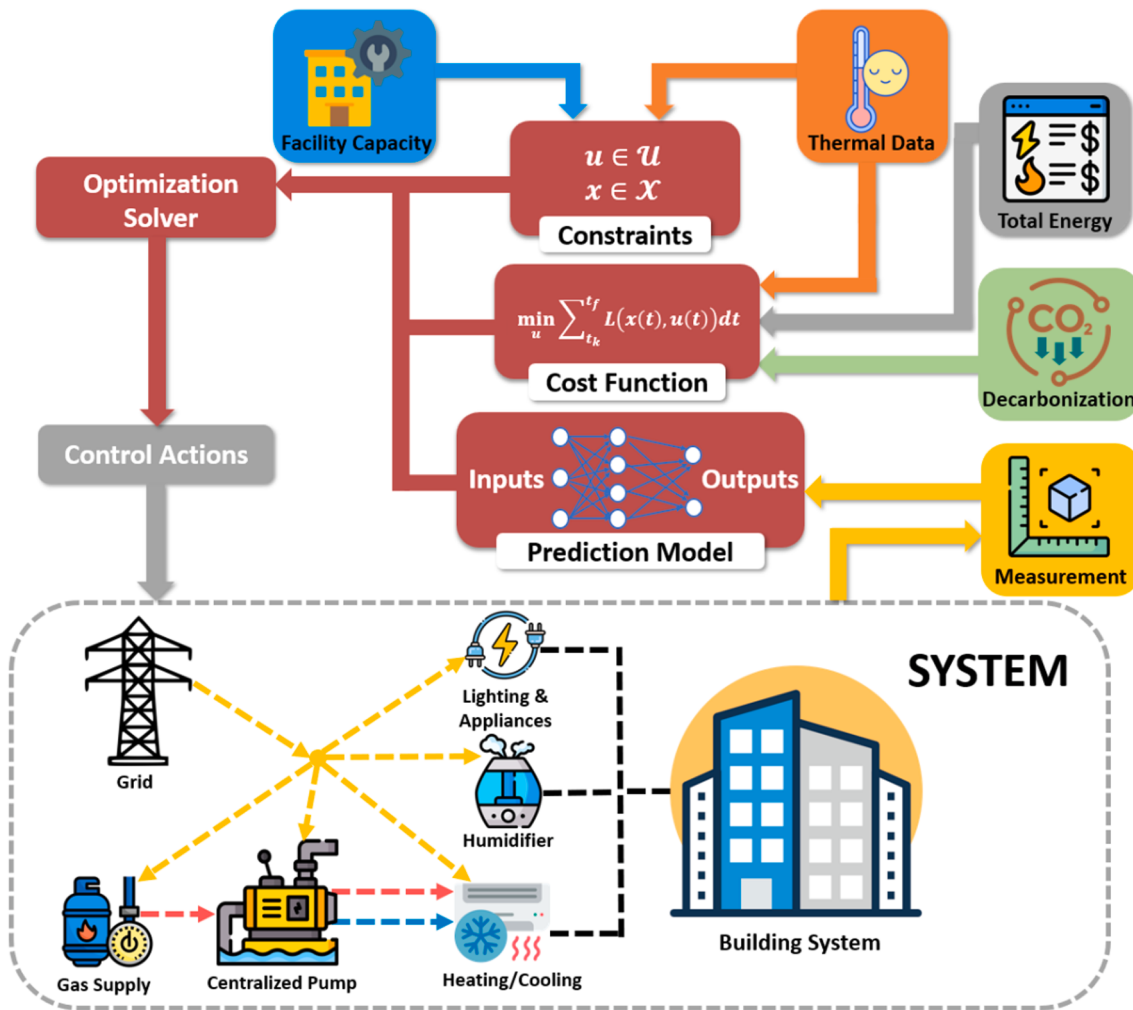


**Fig. 1.** Schematic diagram of the proposed PCDL-based MPC framework for optimizing building energy efficiency and indoor thermal comfort and advancing building decarbonization. Heating and cooling water coils, humidifiers, lighting, and other appliances are included in the building system. Gas centralized pumps are applied to supply hot and chilled water to the coils.

function for building temperature prediction [30]. Another work proposed two unique PiNN models for temperature prediction using a self-defined loss function based on PDEs [31]. Although these models outperformed traditional methods, they lack strict guarantees of physics consistency. The recently proposed physically consistent neural network (PCNN) model proved guarantee of physics consistency under any conditions [32]. Nevertheless, this study only considers a simple single-zone building application case. Moreover, humidity prediction is neglected by all these literatures. Therefore, there is a need for a more comprehensive and generalized physics-informed AI model for indoor temperature and humidity prediction in multi-zone buildings.

The control system is the fundamental component of BEM systems. Controllers fall into two categories: conventional controllers, such as On/Off and proportional integral derivative (PID) controllers, and intelligent controllers, including learning-based [33,34] and model predictive control (MPC) controllers [35,36]. Among these, MPC is more widely researched than other controllers due to its numerous advantages in terms of control performance [37], stability [38,39], and expansibility [40,41]. Most studies adopt physics-based linear state-space models (SSMs), which are effective in certain scenarios [42,43]. However, these models require expert intervention and struggle to handle highly nonlinear and complex systems, which limits their use in real-world applications [37,44]. To address these limitations, researchers have explored data-driven model-based MPC approaches. For instance, random forest regression model-based MPC is used by Hilliard et al. [45]

and Büning et al. [46] for indoor temperature control. The authors of [47] used input convex NN in an MPC framework to control indoor temperature. To optimize energy efficiency and indoor comfort, Yang et al. [48] proposed a machine learning model-based adaptive MPC that outperformed rule-based and linear model-based MPC. However, there is a lack of literature exploring the generalization and data requirement issues of data-driven methods for building control problems. Some researchers have investigated the generalization issues of learning-based methods [49,50] in building energy management problems, proposing self-tuning control methods for optimizing energy efficiency and indoor thermal comfort that showed better generalization ability to different occupant behaviors and weather conditions. Physics-informed AI-based MPC is another effort to address these issues, which has presented great performance than conventional controllers in manipulators [51] and tank reactors [52]. However, the widely used PiNN approach, which relies on a PDE-based loss function, lacks a strict guarantee of physics consistency and requires a high level of expert intervention, hindering its application in MPC. Thus, there is a need for more research exploring the potential use of physics-informed AI models in MPC for building energy management issues.

To fill the aforementioned knowledge gaps, this article proposes a novel physically consistent deep learning (PCDL) modeling method for building thermal modeling and studies its applications in the MPC framework for optimizing building energy efficiency and indoor thermal comfort and advancing building decarbonization. The proposed closed-

**Table 1**

The comparison of previous works on physics-informed AI for building thermal modeling with the proposed work. NN is the neural network; MLP is the multilayer perceptron; LSTM is the long short-term memory model; RC is the resistance–capacitance model; RNN is the recurrent neural network.

Study	Scope		Building Type	Consistency Guarantee	Approach
	Temperature	Humidity			
[30]	✓	✗	Multi-zone	✗	Block NN + Constraints
[31]	✓	✗	Single-zone	✗	MLP + Self-defined Loss function
[32]	✓	✗	Single-zone	✓	LSTM-RC + Constraints
Our work	✓	✓	Multi-zone	✓	LSTM-RNN + Constraints

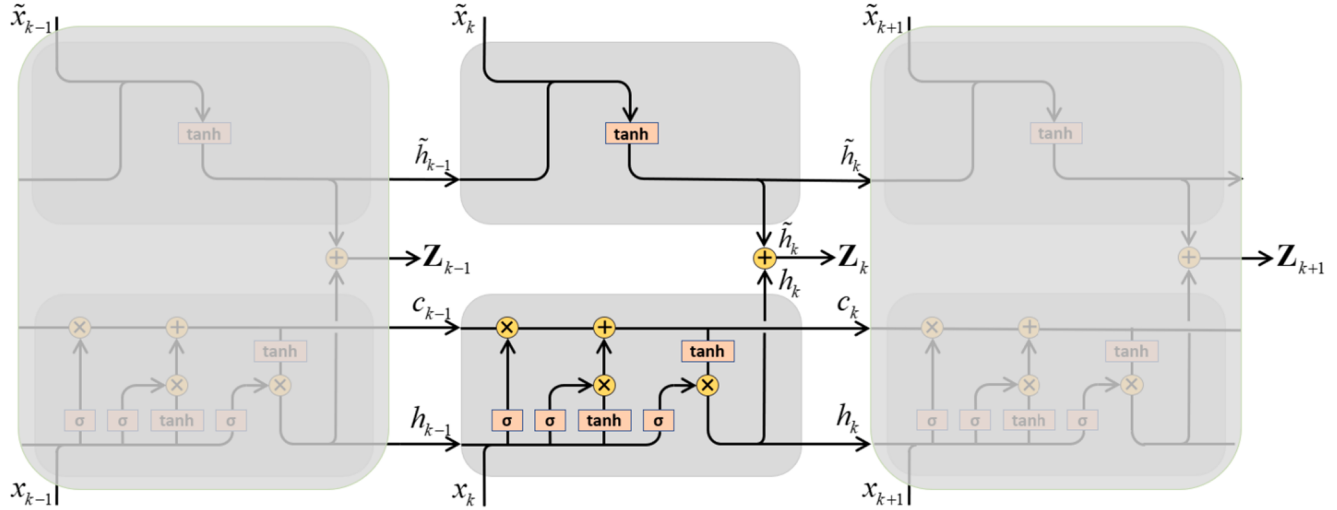


**Fig. 2.** Structure of the PCDL cell, which is a two-layer cell consisting of one RNN cell (top) and one LSTM cell (bottom).  $\sigma$  represents the sigmoid function. The inputs are divided into  $\tilde{x}$  (inputs with physics consistency) and  $x$  (inputs without physics consistency). The final prediction  $Z$  is the summation of  $\tilde{h}$  (the outputs of the RNN cell) and  $h$  (the outputs of the LSTM cell).

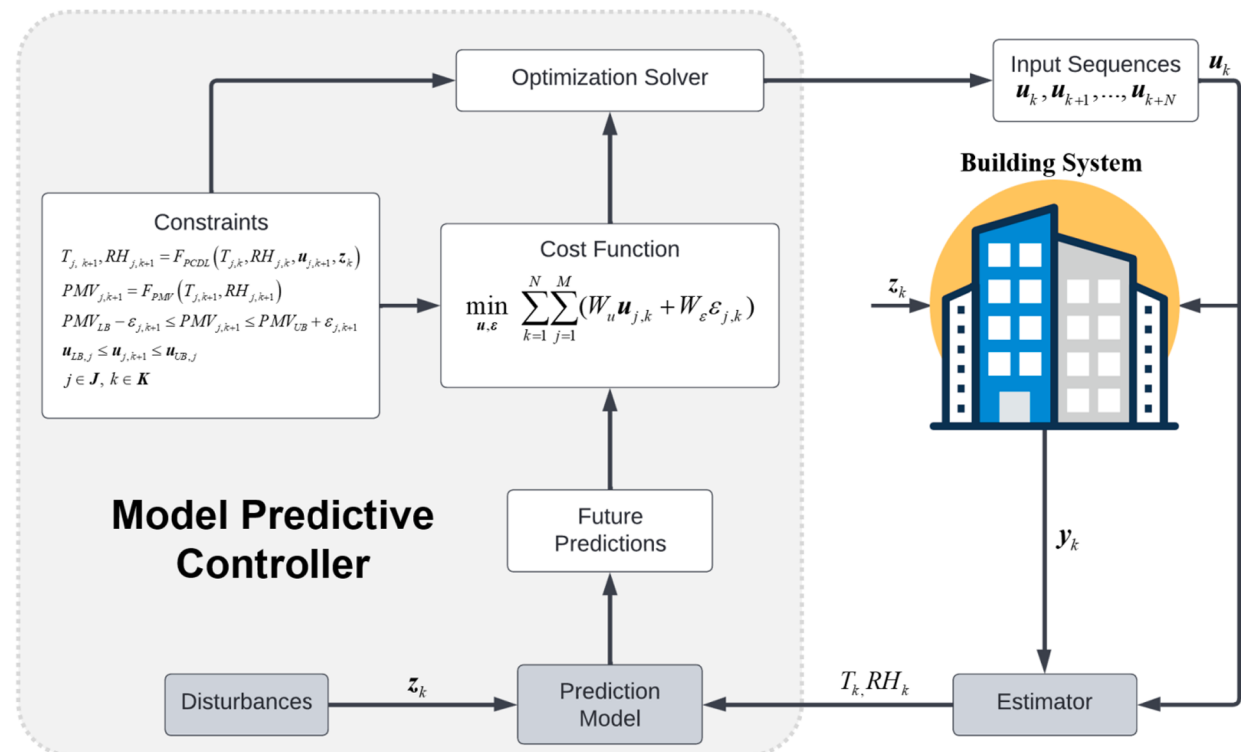


**Fig. 3.** The computing process of the PCDL-based MPC framework.  $y_k$  is the measurement data generated from the building system. The nonlinear optimization problem is recursively solved during the control process.

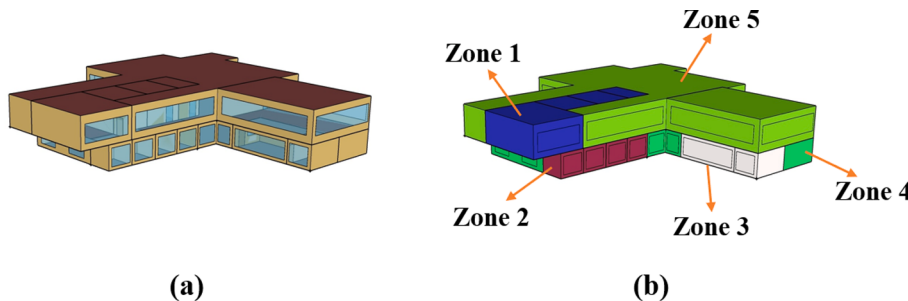


**Fig. 4.** The (a) exterior view and (b) thermal zone division of Carpenter Hall. Each thermal zone is served by one HVAC system to maintain its indoor temperature and humidity.

**Table A1**

The final loss values of the LSTM and the PCDL model.

Model Type	Training Loss	Validation Loss
LSTM	0.004487	0.004260
PCDL	0.008199	0.007924

loop system is depicted in Fig. 1, with the PCDL model serving as the prediction model. The PCDL model features a two-layer structure and parameter constraints based on physics consistencies between building system inputs and outputs. The definition of physics consistencies follows the idea in [32]. Physics consistencies are naturally satisfied using the proposed PCDL model under all conditions. A comparison of physics-informed AI models is presented in Table 1, highlighting the originality of this work. Subsequently, the PCDL model is organically integrated into the MPC controller to predict the indoor temperature and relative humidity with different heating, cooling, and humidifying loads. With relative constraints and objective functions, an optimal control problem is solved iteratively during the control process, balancing energy

efficiency and indoor comfort. Specifically, indoor comfort is evaluated using the predicted mean vote (PMV) index and computed using a linear model based on the predicted temperature and humidity [53]. A case study on a campus building in Cornell University is presented to illustrate the effectiveness and advantages of the proposed PCDL model and the PCDL-based MPC framework for building energy management. Compared to an On/Off controller, an SSM-based MPC controller, and a long short-term memory (LSTM)-based MPC controller, the proposed PCDL-based MPC results in energy savings of 5.8%, 4.5%, and 8.9%, respectively. Furthermore, it improves indoor thermal comfort by 55%, 59%, and 64% compared to these controllers. These results highlight the potential of PCDL-based MPC to contribute to building decarbonization efforts.

The main novelties and contributions of this article are listed as follows:

- A novel PCDL model for the thermal modeling of multi-zone buildings that ensures physics consistency under all conditions and has a

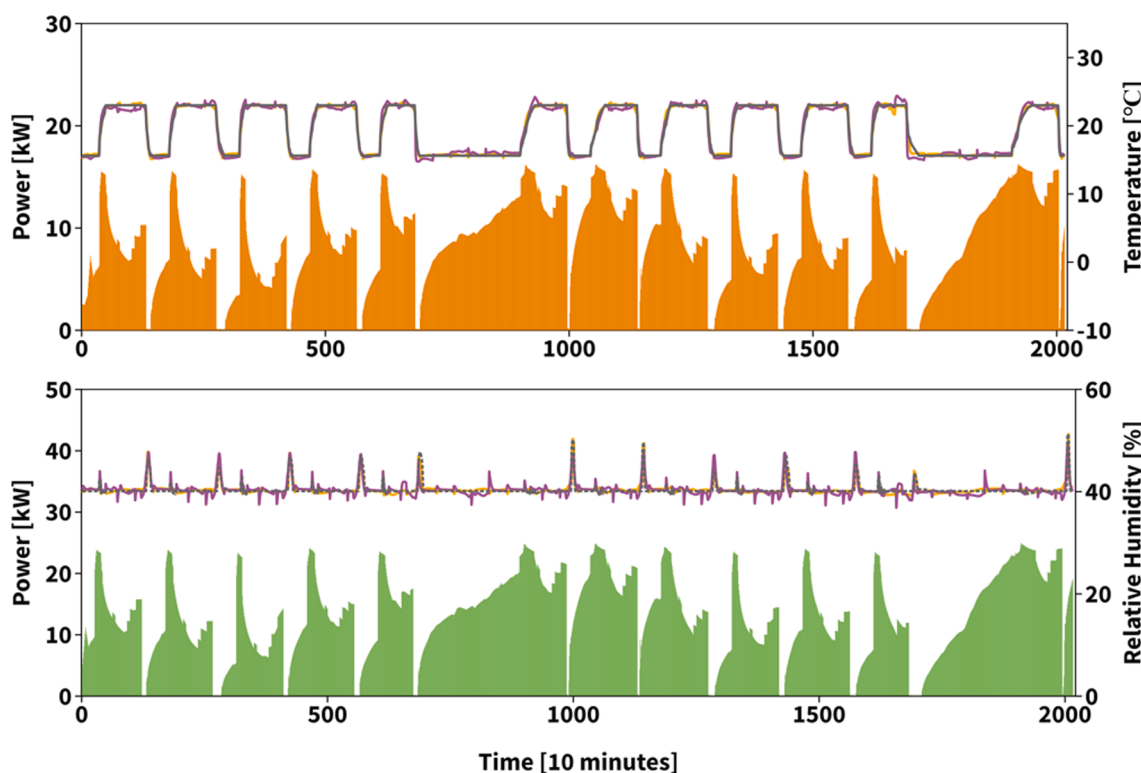


**Fig. 5.** The temperature (top) and relative humidity (bottom) 6-hour prediction results for thermal zone 1. The simulation is conducted from January 1st to 14th, 2022. Yellow lines represent the PCDL prediction results. Purple lines represent the LSTM prediction results. Grey lines are measurement data generated from the EnergyPlus model. (For interpretation of the references to colour in this figure legend, the reader is referred to the web version of this article.)

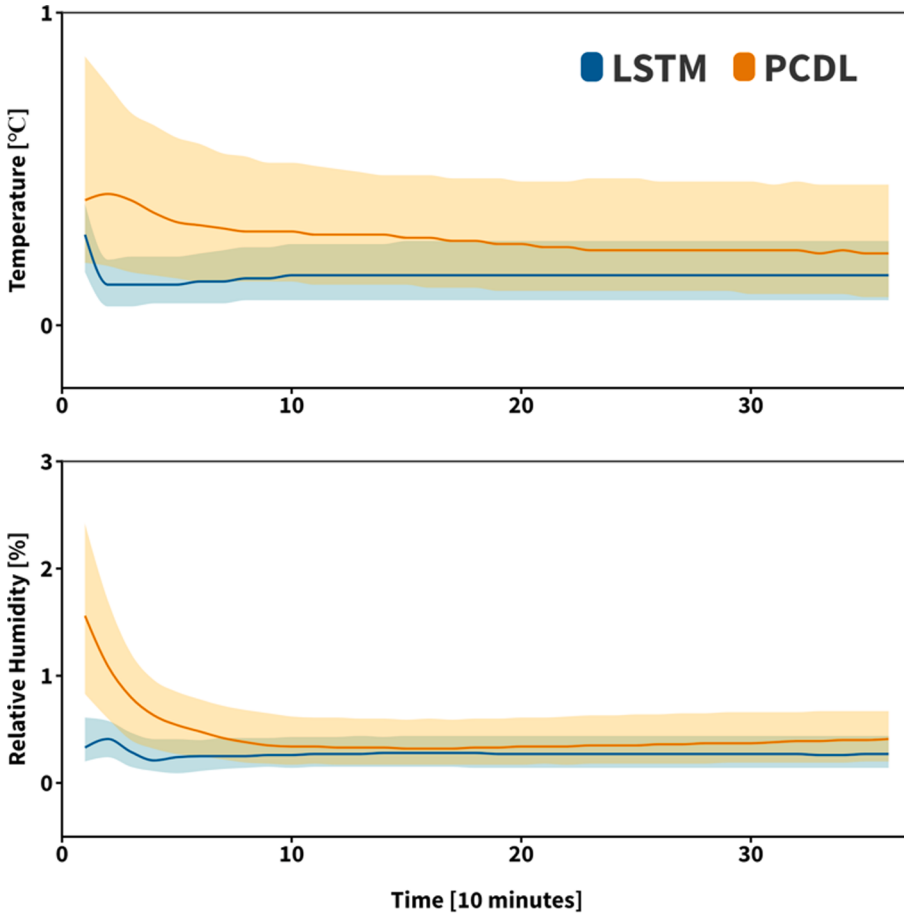


**Fig. 6.** The mean absolute error (MAE) of indoor temperature (top) and relative humidity (bottom) predictions for each prediction interval of the prediction horizon. Yellow lines and shaded areas represent the PCDL prediction MAE values. Blue lines and shaded areas represent the LSTM prediction MAE values. The shaded areas indicate the range between the quarter and three-quarter numbers of the MAE values. (For interpretation of the references to colour in this figure legend, the reader is referred to the web version of this article.)

wider modeling scope and potential applications compared to existing physics-informed AI models for building thermal modeling.

- Demonstrating the superior generalization ability and physics interpretability of the proposed PCDL model compared to the widely adopted LSTM model and emphasizing the significance of these advantages in application to predictive control problems of building energy systems.
- Evaluating the performance of the PCDL model in the MPC framework in comparison to an On/Off controller, an SSM-based MPC controller, and an LSTM-based MPC controller to explore the efficiency and performance limit of physics-informed AI models in the building MPC.

The rest of the article is organized as follows: In [Section 2](#), the definition of physics consistency and the workings of the PCDL model are discussed in detail. [Section 3](#) presents the MPC formulation and its stability and feasibility. The efficacy of the proposed approach is demonstrated through a case study on Carpenter Hall, a building located in Cornell University campus, in [Section 4](#). Finally, the conclusions are summarized in [Section 5](#).

## 2. Physically consistent deep learning model

Building modeling is essential for building design, retrofitting, and control and has been widely used in real-world applications. Of particular importance is building thermal modeling, which is crucial for managing indoor climate and energy consumption in both residential and office buildings. In this section, we introduce a novel PCDL model for building thermal modeling that incorporates prior physics information into its structure and parameters. First, we define the physics consistencies, which outline key relationships between inputs and outputs

in building systems. Then, the PCDL model is constructed using an LSTM cell and a recurrent neural network (RNN) cell. We demonstrate that the physics consistencies are satisfied by adding specific constraints on the RNN weighting parameters.

The proposed physics consistency definitions and LSTM-RNN model structure were inspired by [\[32\]](#), in which the authors used a simplified linear model instead of the RNN cell to approximate physics consistencies of indoor temperature. We have extended this idea in our PCDL model by incorporating physics consistency definitions for humidity and adopting RNN cell to incorporate nonlinear dynamics, enhance the level of physics consistency, and improve the model's approximation ability.

### 2.1. Physics consistency

The thermal dynamics in building systems involve changes in temperature and humidity. In this section, we define key physics consistencies for indoor temperature and relative humidity dynamics. The notion of physics consistency implies that the model should produce physically feasible results in response to any alterations in the specified inputs. The definitions are primarily based on the PCNN method outlined in [\[32\]](#). For example, we can start with the physics consistency definition for indoor temperature and heating power. In accordance with physical laws, we can write the following equation:

$$\frac{\partial T_k}{\partial U_{heat,k-i}} > 0, \quad i = 1, 2, \dots, k-1 \quad (1)$$

where  $T_k$  represents the indoor temperature at timestep  $k$ ,  $U_{heat,k-i}$  represents the heating coil power at timestep  $k-i$ . The above equation shows that an increase in heating power at previous time steps leads to an increase in indoor temperature at the present timestep. Similarly,

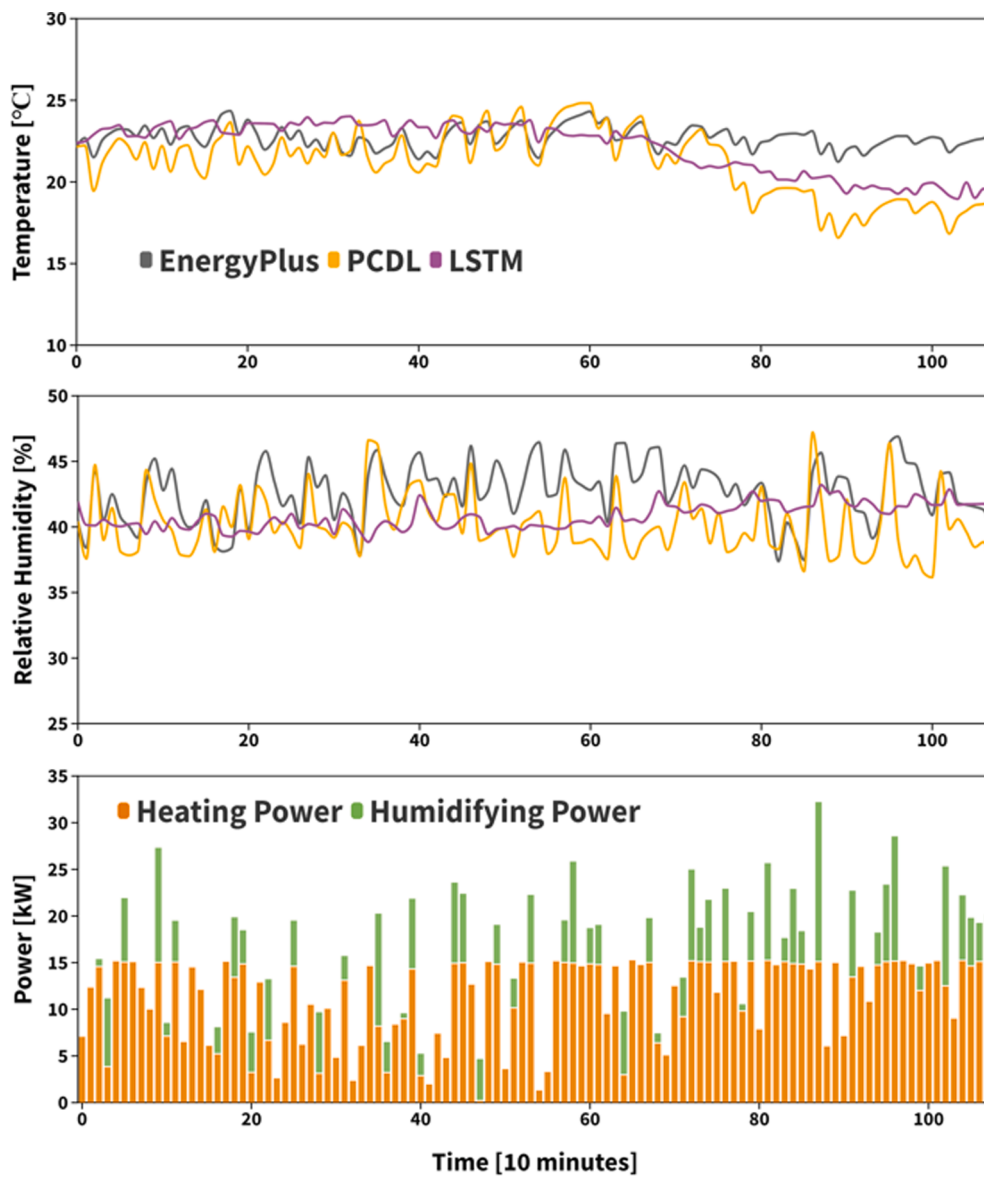


**Fig. 7.** The temperature (top) and relative humidity (middle) prediction results of the PCDL and LSTM models under varying heating and humidifying power (bottom). Grey lines are the results generated from the EnergyPlus model. Yellow lines are the prediction results of the PCDL model. Purple lines are the prediction results of the LSTM model. (For interpretation of the references to colour in this figure legend, the reader is referred to the web version of this article.)

additional physics consistencies can be derived for indoor temperature and humidity as follows:

$$\frac{\partial T_k}{\partial U_{cool,k-i}} < 0, \quad i = 1, 2, \dots, k-1 \quad (2)$$

$$\frac{\partial T_k}{\partial T_{e,k-i}} > 0, \quad i = 1, 2, \dots, k-1 \quad (3)$$

$$\frac{\partial T_k}{\partial T_{ne,k-i}} > 0, \quad i = 1, 2, \dots, k-1 \quad (4)$$

$$\frac{\partial RH_k}{\partial U_{hum,k-i}} > 0, \quad i = 1, 2, \dots, k-1 \quad (5)$$

$$\frac{\partial RH_k}{\partial RH_{e,k-i}} > 0, \quad i = 1, 2, \dots, k-1 \quad (6)$$

$$\frac{\partial RH_k}{\partial RH_{ne,k-i}} > 0, \quad i = 1, 2, \dots, k-1 \quad (7)$$

$$\frac{\partial RH_k}{\partial T_{k-i}} > 0, \quad i = 1, 2, \dots, k-1 \quad (8)$$

where  $U_{cool,k-i}$  is the cooling power at timestep  $k-i$ ;  $T_{e,k-i}$  is the outdoor environment temperature at timestep  $k-i$ ;  $T_{ne,k-i}$  refers to the temperature of both the neighbor zone and the considered zone at timestep  $k-i$ ;  $RH_k$  is the relative humidity at timestep  $k$ ;  $U_{hum,k-i}$  is the humidifier power at timestep  $k-i$ ;  $RH_{e,k-i}$  is the outdoor environment relative humidity at timestep  $k-i$ ;  $RH_{ne,k-i}$  refers to the relative humidity of both the neighbor zone and the considered zone at timestep  $k-i$ . Inequalities (1) to (8) define the inputs of the building thermal model that incorporate physics consistency. Specifically, inequality (8) defines the relationship between relative humidity and indoor temperature. Additional physics consistencies, such as solar irradiances and occupant's radiant energy, can be defined through the same method. However, in this work, these factors were not considered because they have a lesser impact on indoor temperature and humidity than the inputs specified in inequalities (1) to (8).

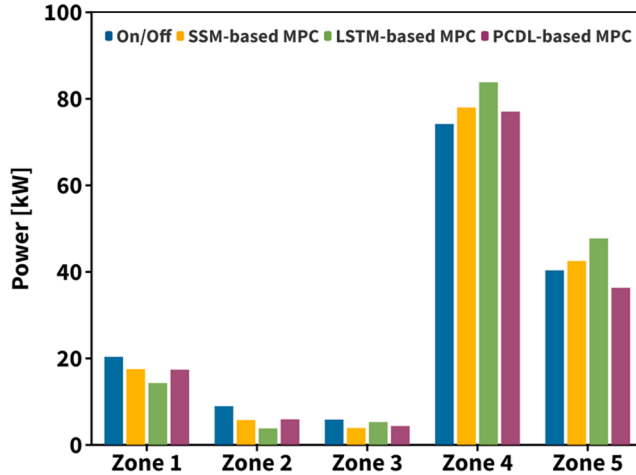


**Fig. 8.** The average power consumption of each thermal zone by using the On/Off controller, SSM-based MPC controller, LSTM-based MPC controller, and the proposed PCDL-based MPC controller.

## 2.2. PCDL model architecture

The proposed PCDL model consists of a two-layer NN: an LSTM cell and an RNN cell, as shown in Fig. 2. The inputs with physics consistency, including the heating power, cooling power, humidifying power, outdoor temperature, and outdoor relative humidity, are fed into the RNN cell (represented by  $\tilde{x}$ ). The inputs without physics consistency, including the number of occupants in every zone, solar irradiances, and time information, are fed into the LSTM cell (represented by  $x$ ).  $Z$  represents the prediction results, which is the sum of the outputs from the RNN cell ( $\tilde{h}$ ) and the LSTM cell ( $h$ ). The subscript  $k$  represents the corresponding timestep. The initial hidden state for the RNN cell is the output ( $\tilde{h}$ ) from the last time step. Moreover, the initial hidden state and cell state for the LSTM cell is the output ( $h$ ) and the cell output ( $c$ ) from the previous timestep. For the first timestep, the initial hidden state of

the RNN cell is the indoor temperature and humidity values measured from the building system. The initial states of the LSTM cell are all-zero vectors with appropriate dimensions.

The presented model structure is designed specifically for building thermal modeling. The sigmoid and tanh functions in the cell are used to capture the nonlinear thermal dynamics. Moreover, the defined-NN structure can largely improve the approximation ability of the PCDL model compared to the traditional RC model. The two-layer structure, consisting of an LSTM cell and an RNN cell, separates physically consistent inputs and other inputs. The RNN cell ensures physics consistency through pre-defined parameter constraints, while the LSTM cell captures unmodeled dynamics and improves long-term prediction accuracy. The PCDL model is trained using a tailored warm-up method, as described in Section A1 of the Appendix.

It is worth noting that the use of LSTM cells, which are considered as an advanced version of RNNs, was not deemed suitable for capturing physics consistency for two primary reasons. Firstly, the definition of physics consistency guarantee for LSTM cells is rather complicated due to the Hadamard product employed in the LSTM computation process. Secondly, the physics consistencies defined based on the thermal dynamics of buildings have limited long-term dynamics, indicating that using RNNs can be sufficient for capturing these dynamics.

## 2.3. Physics consistency guarantee

All considered physics consistencies can be defined by adding additional constraints on the RNN cell parameters. Details are presented via the derivations below. Specifically, the process of computation in the RNN cell can be written as follows:

$$\tilde{h}_k = \tanh \left( \tilde{x}_k W_{ih}^T + b_{ih} + h_{k-1} W_{hh}^T + b_{hh} \right) \quad (9)$$

where  $W_{ih}^T$  and  $W_{hh}^T$  are weighting parameters for inputs  $\tilde{x}_k$  and initial states  $\tilde{h}_{k-1}$ , respectively;  $b_{ih}$  and  $b_{hh}$  are bias parameters for inputs  $\tilde{x}_k$  and initial states  $\tilde{h}_{k-1}$ , respectively. Without loss of generality, we can assume  $\tilde{x}_k$  and  $\tilde{h}_{k-1}$  to be one-dimensional, representing a single-input

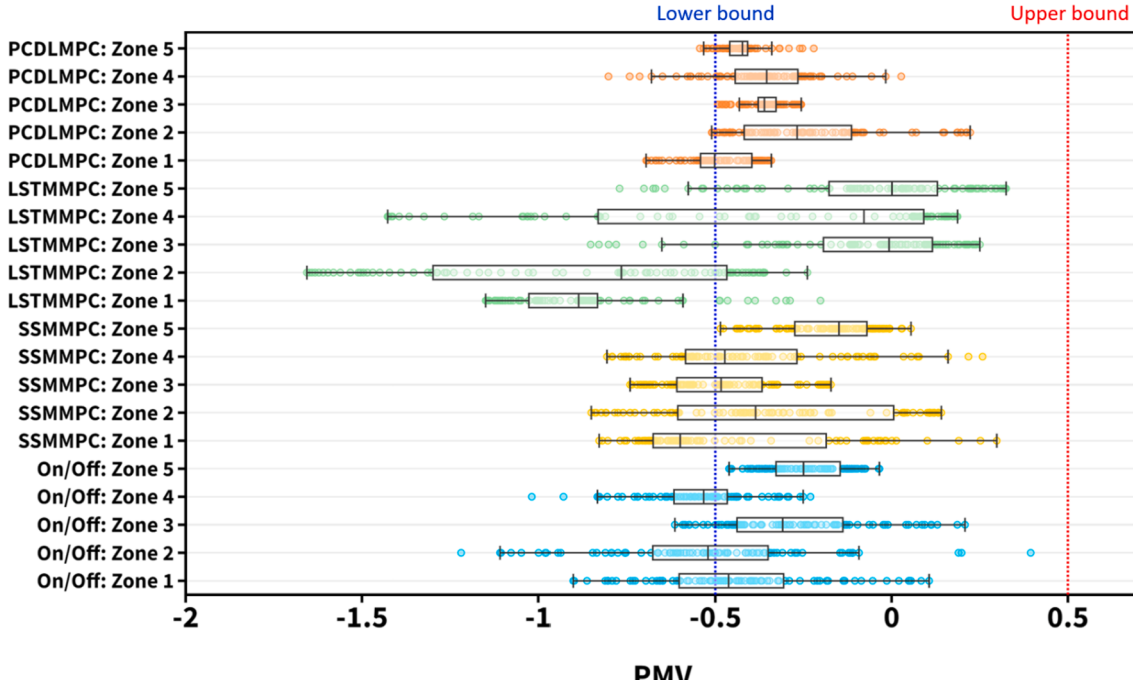


**Fig. 9.** Statistical PMV distributions of each thermal zone by using the On/Off controller, SSMMPC controller (SSMMPC), LSTMMPC controller (LSTMMPC), and the proposed PCDLMPC controller (PCDLMPC). The dashed lines represent the lower and upper bounds of PMV.

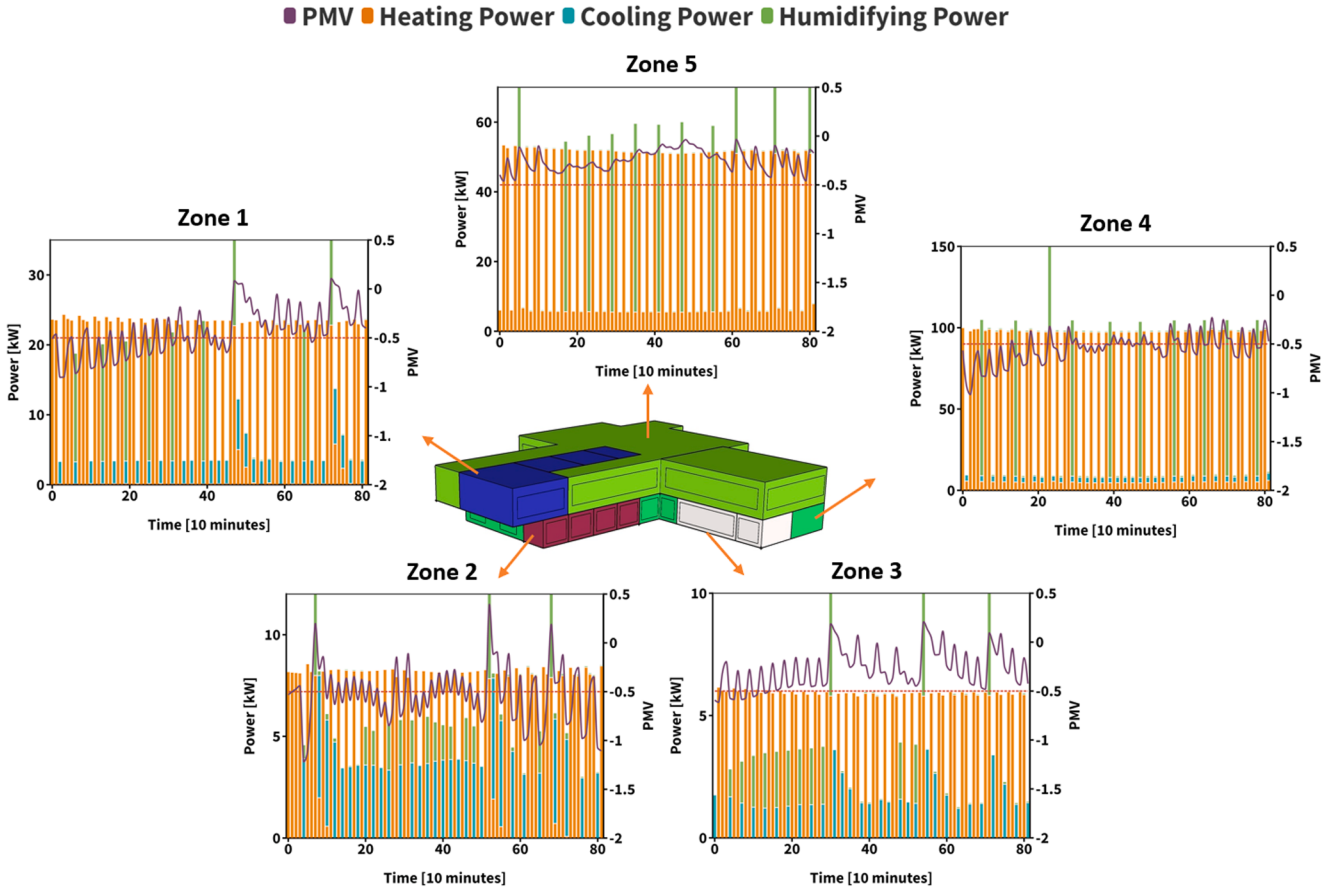


**Fig. 10.** The PMV level and energy consumption profiles from 8:00 to 22:00 on January 15th by using the On/Off controller. The purple lines are the PMV control profiles. The red dash lines are the lower bounds for PMV values. The orange, blue, and green columns are the heating, cooling, and humidifying power consumption, respectively. (For interpretation of the references to colour in this figure legend, the reader is referred to the web version of this article.)

single-output (SISO) system. Therefore, the weighting and bias parameter matrices become scalars. It should be noted that the derivation in this section can be easily extended to multiple-input multiple-output (MIMO) systems as well.

The derivative of  $\tilde{h}_k$  with respect to the input  $\tilde{x}_{k-i}$  can be written as the following:

$$\frac{\partial \tilde{h}_k}{\partial \tilde{x}_{k-i}} = TD \cdot W_{hh}^i \cdot W_{ih}, \quad i = 1, 2, \dots, k-1 \quad (10)$$

where  $TD$  is the product of  $i+1$  derivatives of the tanh function. Specifically, the tanh function and its derivative are given as follows:

$$y = \tanh(x) = \frac{e^x - e^{-x}}{e^x + e^{-x}} \quad (11)$$

$$\frac{dy}{dx} = 1 - \left( \frac{e^x - e^{-x}}{e^x + e^{-x}} \right)^2 \quad (12)$$

It can be inferred that the  $TD$  term is always positive since every derivative of the tanh function is positive if  $x$  is finite. Therefore, if we have the following constraints for  $W_{ih}$  and  $W_{hh}$ :

$$W_{ih} > 0, \quad W_{hh} > 0 \quad (13)$$

Combined with Eq. (10), we have the inequality as follows:

$$\frac{\partial \tilde{h}_k}{\partial \tilde{x}_{k-i}} = TD \cdot W_{hh}^i \cdot W_{ih} > 0, \quad i = 1, 2, \dots, k-1 \quad (14)$$

From the two-layer model structure, the following equations can be easily derived:

$$\mathbf{Z}_k = \tilde{h}_k + h_k \quad (15)$$

$$\frac{\partial h_k}{\partial \tilde{x}_{k-i}} = 0, \quad i = 1, 2, \dots, k-1 \quad (16)$$

Then the physics consistency definition is written by using Eqs. (14) to (16):

$$\frac{\partial \mathbf{Z}_k}{\partial \tilde{x}_{k-i}} = \frac{\partial \tilde{h}_k}{\partial \tilde{x}_{k-i}} + \frac{\partial h_k}{\partial \tilde{x}_{k-i}} = TD \cdot W_{hh}^i \cdot W_{ih} > 0, \quad i = 1, 2, \dots, k-1 \quad (17)$$

To define negative physics consistency, such as the cooling power, we can simply transform the corresponding inputs  $\tilde{x}$  to  $-\tilde{x}$  and apply the same definition as previously discussed. However, the above definition does not cover the considered inputs  $T_{ne}$ ,  $RH_{ne}$ , and  $T_{k-i}$ , which are included in  $\mathbf{Z}$  rather than  $\tilde{x}$ . Following the same SISO assumption, the derivative of  $\mathbf{Z}_k$  with respect to  $\mathbf{Z}_{k-i}$  can be written as the following equation:

$$\frac{\partial \mathbf{Z}_k}{\partial \mathbf{Z}_{k-i}} = \frac{\partial \tilde{h}_k}{\partial \mathbf{Z}_{k-i}} + \frac{\partial h_k}{\partial \mathbf{Z}_{k-i}} = \frac{\partial \tilde{h}_k}{\partial \tilde{h}_{k-i}} + \frac{\partial h_k}{\partial h_{k-i}}, \quad i = 1, 2, \dots, k-1 \quad (18)$$

Because the inputs  $x_k$  and initial states  $h_{k-1}$  are not modified during the control process, the output  $h_k$  of the LSTM cell can be treated to be constant. Therefore, the following equation can be written:

$$\frac{\partial h_k}{\partial h_{k-i}} = 0, \quad i = 1, 2, \dots, k-1 \quad (19)$$

Based on Eq. (9), the derivative of  $\tilde{h}_k$  with respect to  $\tilde{h}_{k-i}$  can be written as follows:

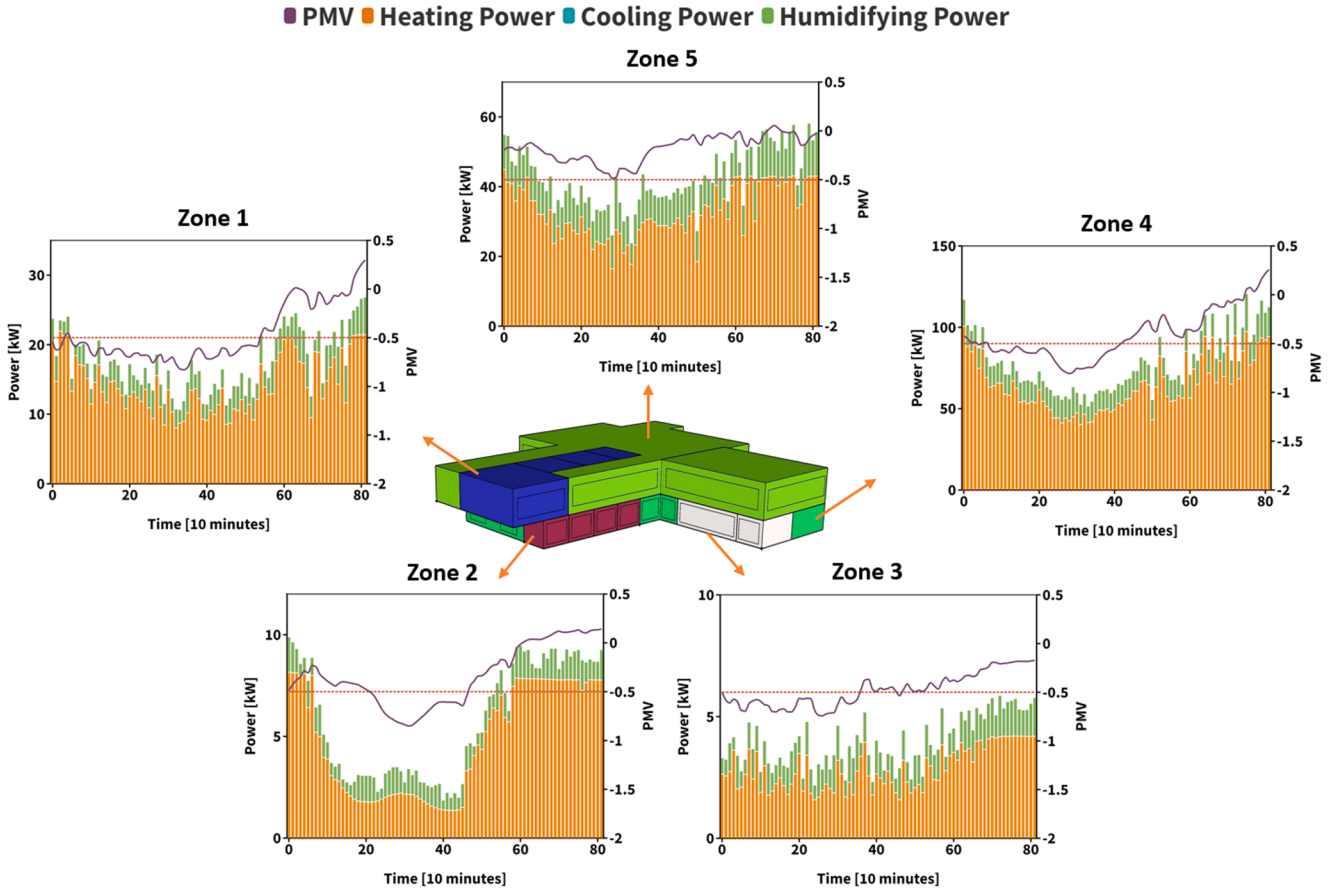


**Fig. 11.** The PMV level and energy consumption profiles from 8:00 to 22:00 on January 15th by using the SSM-based MPC controller. The purple lines are the PMV control profiles. The red dash lines are the lower bounds for PMV values. The orange, blue, and green columns are the heating, cooling, and humidifying power consumption, respectively. (For interpretation of the references to colour in this figure legend, the reader is referred to the web version of this article.)

$$\frac{\partial \tilde{h}_k}{\partial h_{k-i}} = TD \cdot W_{hh}^{i+1} > 0, \quad i = 1, 2, \dots, k-1 \quad (20)$$

Then Eqs. (19) and (20) can be substituted into Eq. (18) and the following inequality is written:

$$\frac{\partial Z_k}{\partial Z_{k-i}} = TD \cdot W_{hh}^{i+1} > 0, \quad i = 1, 2, \dots, k-1 \quad (21)$$

Therefore, the above inequality defines the physics consistency of the state inputs, such as  $T_{ne}$ ,  $RH_{ne}$ , and  $T_{k-i}$ . By combining Eqs. (17) and (21), this section proves that all the physics consistencies considered in Section 2.1 can be ensured with the parameter constraints defined in inequality (13).

### 3. PCDL-based model predictive control

After constructing the PCDL model, we then present the PCDL-based MPC framework for building systems. The PCDL-based MPC is designed to optimize energy efficiency and regulate indoor thermal comfort concurrently and can be utilized in typical office or residential buildings. The framework starts with a presentation of the control system, followed by discussions of its stability and feasibility. By utilizing the PCDL model, the framework is able to make energy-efficient decisions while ensuring indoor thermal comfort at the same time.

#### 3.1. PCDL-based control framework

The PCDL model predicts the indoor temperature and humidity, and the prediction can be written as the following:

$$[T_{j-k+1}, RH_{j,k+1}] = F_{PCDL}(T_{j,k}, RH_{j,k}, u_{j,k}, z_k) \quad (22)$$

where subscript  $j$  and  $k$  are the corresponding zone number and timestep, respectively. The control input  $u$  includes heating power, cooling power, and humidifying power. Disturbance input  $z$  includes ambient temperature, ambient humidity, number of occupants in each zone, solar irradiances, and time information.  $F_{PCDL}$  represents the PCDL model, which is a nonlinear function.

The PMV index is computed from the predicted temperature and relative humidity by using a linear model. The details of the simplified PMV model generation can be found in Section A2 of the Appendix. The PMV index is used to quantify indoor thermal comfort and is calculated as follows:

$$PMV_{j,k+1} = F_{PMV}(T_{j,k+1}, RH_{j,k+1}) \quad (23)$$

where  $F_{PMV}$  is the generated linear model for PMV estimation.

The upper and lower bounds for the PMV index are defined to maintain comfortable indoor environments. These bounds are expressed using the following inequalities:

$$PMV_{LB} - \epsilon_{j,k+1} \leq PMV_{j,k+1} \leq PMV_{UB} + \epsilon_{j,k+1} \quad (24)$$

$PMV_{LB}$  and  $PMV_{UB}$  represent the lower and upper bounds for the PMV index, respectively.  $\epsilon_{j,k+1}$  is the defined slack variable for constraint violation, which is used to guarantee the optimization problem feasibility.

For physical limitation considerations, the constraints for control inputs are also needed to be considered, which can be written as:

$$u_{LB,j} \leq u_{j,k+1} \leq u_{UB,j} \quad (25)$$

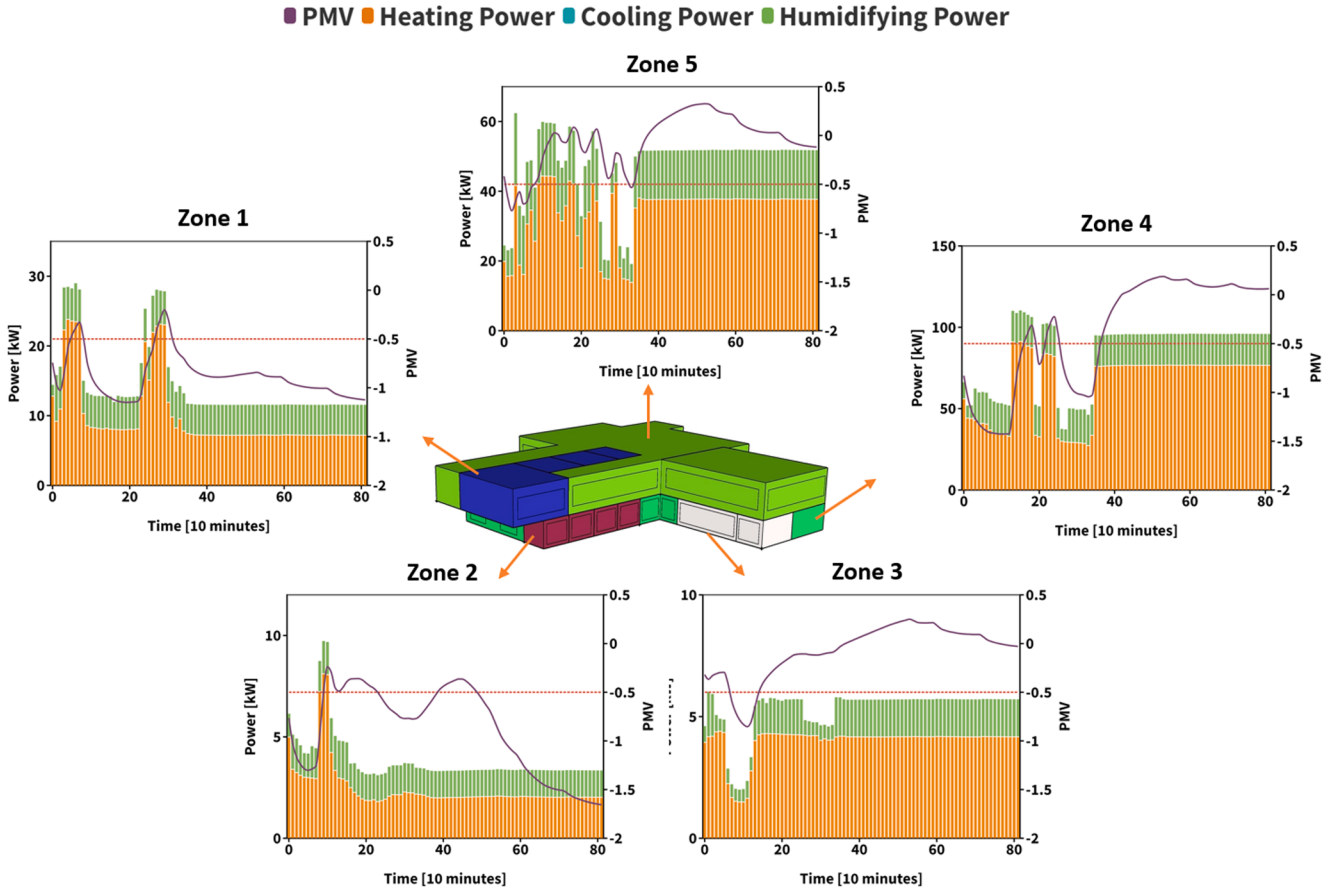


**Fig. 12.** The PMV level and energy consumption profiles from 8:00 to 22:00 on January 15th by using the LSTM-based MPC controller. The purple lines are the PMV control profiles. The red dash lines are the lower bounds for PMV values. The orange, blue, and green columns are the heating, cooling, and humidifying power consumption, respectively. (For interpretation of the references to colour in this figure legend, the reader is referred to the web version of this article.)

$u_{LB}$  and  $u_{UB}$  represent the lower and upper bounds for the control inputs, which include the heating power, cooling power, and humidifying power.

Subsequently, the nonlinear optimization problem is formulated based on the defined dynamic models and constraints for the predictive control system:

$$\begin{aligned} \min_{\mathbf{u}, \mathbf{e}} & \sum_{k=1}^N \sum_{j=1}^M (W_u \mathbf{u}_{j,k-1} + W_e \mathbf{e}_{j,k}) \\ \text{s.t. } & T_{j,k+1}, RH_{j,k+1} = F_{PCDL}(T_{j,k}, RH_{j,k}, \mathbf{u}_{j,k}, z_k) \\ & PMV_{j,k+1} = F_{PMV}(T_{j,k+1}, RH_{j,k+1}) \\ & PMV_{LB} - \epsilon_{j,k+1} \leq PMV_{j,k+1} \leq PMV_{UB} + \epsilon_{j,k+1} \\ & u_{LB,j} \leq \mathbf{u}_{j,k} \leq u_{UB,j} \\ & j \in J = \{1, 2, \dots, M\}, \quad k \in K = \{0, 1, \dots, N-1\} \end{aligned} \quad (26)$$

where  $W_u$  and  $W_e$  represent the weighting parameters for the control inputs and slack variables. Therefore, the objective function is defined to minimize energy consumption and indoor comfort violations concurrently.  $M$  is the total number of zones, and  $N$  is the prediction horizon length. The initial data  $T_{j,0}$  and  $RH_{j,0}$  are obtained from the measurements of the building system. Specifically, the nonlinear optimization problem can be solved by using nonlinear programming solvers, like IPOPT and CONOPT. More details of the PCDL-based MPC are presented in Section 4.3.

The defined nonlinear optimization problem is recursively solved during the control process, which is presented in Fig. 3. At every time-step, the initial indoor temperature and humidity are determined using the state estimator and real-time measurements  $y_k$ , which are combined with disturbances  $z_k$  to produce future predictions using the prediction

model. Then the optimization problem is solved with the cost function and constraints and only the first control action  $u_k$  is applied to the building system. This process is repeated until the final timestep is reached.

### 3.2. Feasibility and stability of the PCDL-based MPC framework

For MPC systems, feasibility and stability are two important issues that need to be addressed before applications in the real world. Feasibility refers to the absence of infeasible solutions under changing inputs and disturbances. On the other hand, stability refers to the requirement for bounded outputs and states with bounded inputs, which is crucial for system safety.

To ensure feasibility in MPC systems, soft constraints and slack variables are commonly used [56,57]. In this work, we introduce soft constraints for the PMV upper and lower bounds, and the objective function minimizes the corresponding slack variables. The advantage of using soft constraints over hard constraints is that they can be satisfied in any condition by allowing for sufficiently large slack variables.

The stability of the proposed PCDL-based MPC framework can be proved following the previous stability research on nonlinear MPC controllers [58–61]. Specifically, the asymptotic stability of a given nonlinear MPC controller can be guaranteed if the following assumptions are satisfied:

**Assumption 1.** The system dynamic function  $f(\mathbf{x}, \mathbf{u}) : \mathbb{R}^n \times \mathbb{R}^m \rightarrow \mathbb{R}^n$  is twice continuous differentiable.

**Assumption 2.** The input region  $U \subset \mathbb{R}^m$  is compact and convex, and the origin  $\mathbf{u}_0 \in U$ .

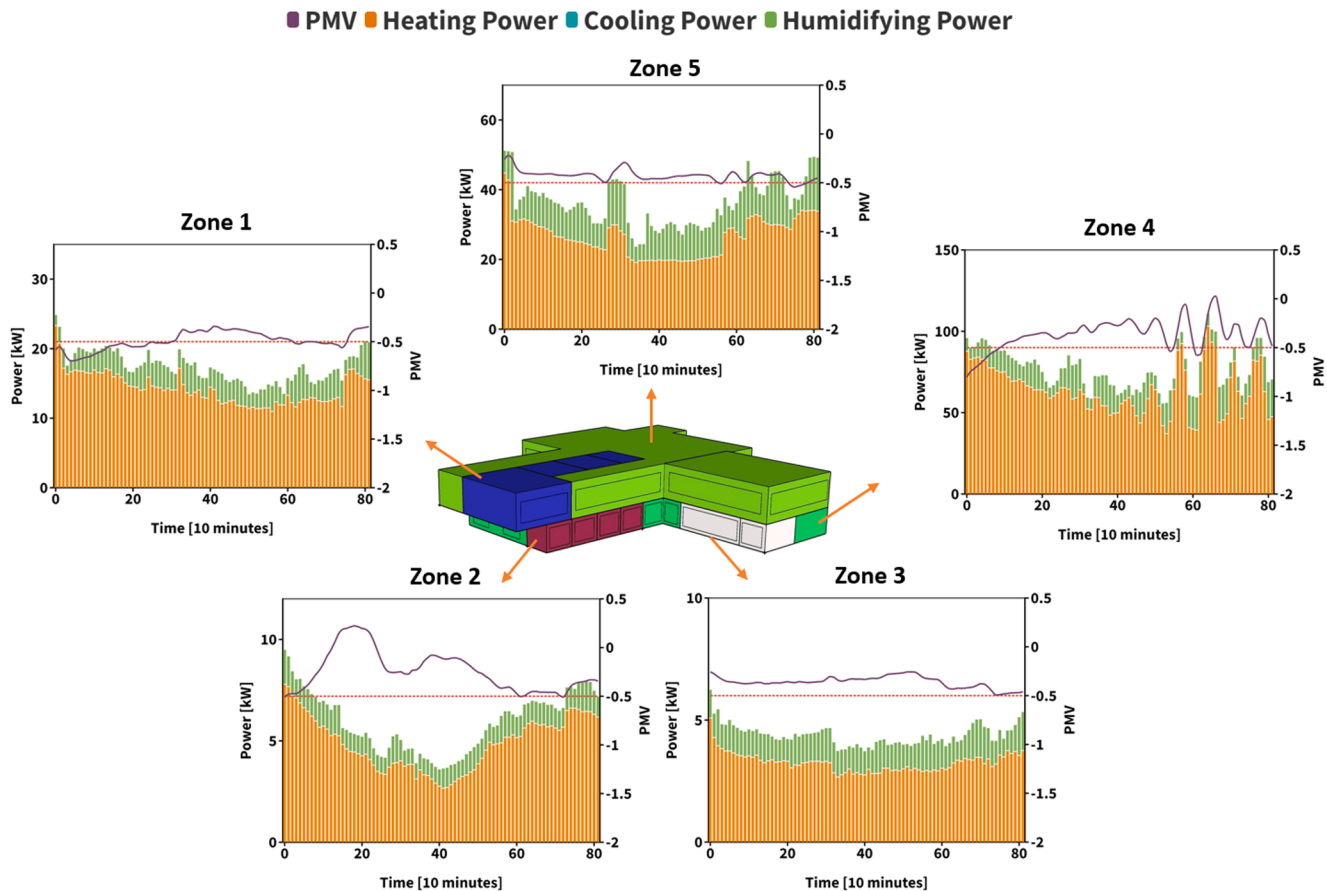


**Fig. 13.** The PMV level and energy consumption profiles from 8:00 to 22:00 on January 15th by using the proposed PCDL-based MPC controller. The purple lines are the PMV control profiles. The red dash lines are the lower bounds for PMV values. The orange, blue, and green columns are the heating, cooling, and humidifying power consumption, respectively. (For interpretation of the references to colour in this figure legend, the reader is referred to the web version of this article.)

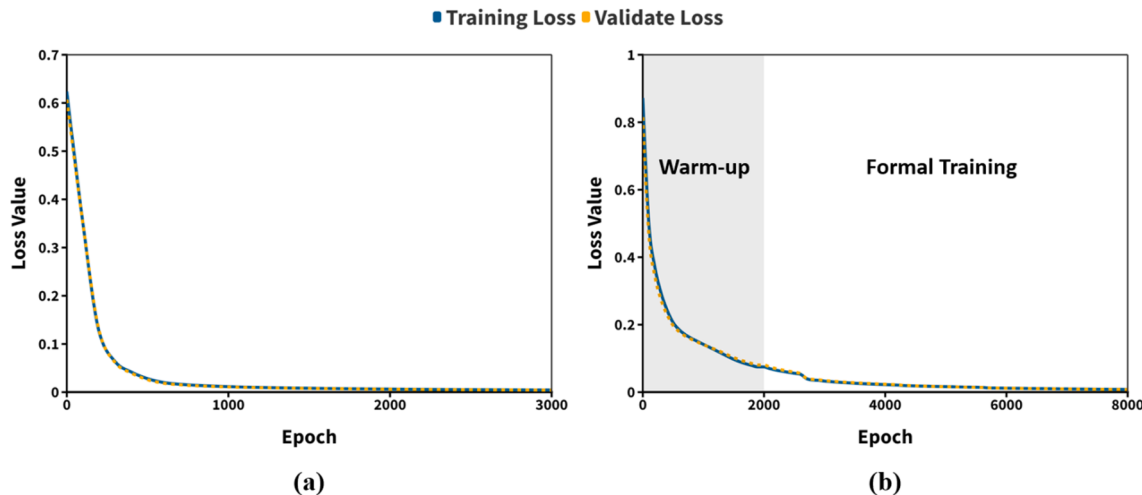


**Fig. A1.** The training and validation loss profiles of (a) the LSTM model and (b) the PCDL model. The solid blue lines represent the training loss. The dashed yellow lines represent the validation loss.

**Assumption 3.** The open-loop optimal control problem is feasible at time  $t = 0$ .

**Assumption 4.** The system dynamic function's Jacobian linearization  $\dot{x} = Ax + Bu$  within the feasible region is stabilizable, where  $A := \left. \frac{\partial f}{\partial x} \right|_{(x,u)}$  and  $B := \left. \frac{\partial f}{\partial u} \right|_{(x,u)}$ .

In the above assumptions,  $n$  and  $m$  represent the dimensions of the system states and inputs;  $x$  and  $u$  represent the system states and inputs;  $u_0$  represent the origin of  $u$ . Subsequently, we check the above assumptions with the proposed PCDL-based MPC framework. **Assumption 1** is satisfied by the PCDL model due to the use of the tanh and sigmoid functions, which are twice continuously differentiable. **Assumption 2** is satisfied by the box constraints defined in Eq. (25). The feasibility of the

proposed control framework is ensured through soft constraints, fulfilling the requirements of [Assumption 3](#). To verify assumption 4, we first write the following lemma.

**Lemma 1. (Hautus Lemma)** Given real matrices  $A \in M_{n \times n}$  and  $B \in M_{n \times m}$ , the matrix pair  $(A, B)$  is stabilizable if and only if it satisfies:

$$\text{rank}[\lambda I - A, B] = n, \quad \forall \lambda \in \{\lambda | \lambda \in \Lambda, \text{Re}(\lambda) \geq 0\} \quad (27)$$

where  $\Lambda$  is the set of all eigenvalues of  $A$ . The proof of the above lemma can be found in [62]. Therefore, we can claim that if the Jacobian linearization of the PCDL model satisfies Eq. (27), [Assumption 4](#) will be satisfied. Specifically, we can write the Jacobian linearization of the PCDL model within the feasible region as follows:

$$A_{PCDL} = \frac{\partial F_{PCDL}}{\partial u} \Big|_{(x,u)} = TD_{(x,u)} \cdot W_{ih,u}^T \quad (28)$$

$$B_{PCDL} = \frac{\partial F_{PCDL}}{\partial Z} \Big|_{(x,u)} = TD_{(x,u)} \cdot W_{hh}^T \quad (29)$$

$u$  includes heating, cooling, and humidifying power of all zones;  $Z$  includes the temperature and humidity of all zones.  $TD_{(x,u)}$  is the corresponding derivative of the tanh function.  $W_{ih,u}^T$  is part of  $W_{ih}^T$  and represents the corresponding weighting parameters for inputs  $u$ .

To summarize, the PCDL-based MPC is guaranteed to have asymptotic stability provided that  $A_{PCDL}$  and  $B_{PCDL}$  meet the conditions outlined in Eq. (27). It should be noted that the stability guarantee of disturbances  $z$  is not illustrated in this section, considering we assume perfect predicted disturbances in this work.

#### 4. Application to the Carpenter Hall in Cornell University campus

##### 4.1. System and simulation description

The proposed PCDL-based thermal modeling method is applied to the Carpenter Hall in Cornell University campus, Ithaca, New York, which is a two-floor office building currently used by the College of Engineering. [Fig. 4](#) shows the exterior view of Carpenter Hall, which has a total area of 2,785 m<sup>2</sup> and total volume of 13,606 m<sup>3</sup>, respectively. The building constructions (e.g., walls, doors, windows) and operating conditions (e.g., facilities, occupants, schedules) are defined based on the ASHRAE standard [63]. The building is divided into five thermal zones, as depicted in [Fig. 4](#). Each thermal zone is served by a heating, ventilation, and air conditioning (HVAC) system consisting of one heating water coil, one cooling water coil, one humidifier, one outdoor air system, and several fans. The hot and chilled water is supplied by district sources powered by gas. The historical weather and solar irradiances data is obtained from an open-source dataset [64] and used in the simulation and control process.

The simulation model is constructed in EnergyPlus, a tool with flexible building definitions and convenient interfaces for co-simulation with other tools. Considering the harsh winter in Ithaca, the simulation period selected is January, which is typically the coldest month in Ithaca. Specifically, the simulation is conducted from January 1st to 14th, 2022. The simulation data is sampled every 10 min during the simulation process, which is used to train the PCDL model and a two-layer LSTM model for comparison. The PCDL and LSTM models are constructed in Python using PyTorch. An SSM is also developed by implementing the building resistance-capacitance model (BRCM) toolbox for comparison [65]. The time interval for all the models is set to be 10 min. The modeling process of the SSM is presented in Section A3 of the Appendix. Besides, the PCDL-based MPC, LSTM-based MPC, SSM-based MPC, and an On/Off controller are established by employing the Building Controls Virtual Test Bed toolbox [66], which links MATLAB and EnergyPlus for co-simulation. The control time interval is 10

min, and the prediction horizon is 6 h. The optimization problems are solved in Python using the IPOPT solver, which is suitable for solving large-scale nonlinear optimization problem, and the computational results are sent back to MATLAB. Optimization problems are solved in parallel with different initial points to overcome the local optimality issue by selecting the best solution. The simulation and computation are conducted on a desktop with an Intel Core i9-13900 K processor at 5.4 GHz and 128 GB of RAM. The average time required to solve the optimization problem in the SSM-based, LSTM-based, and PCDL-based MPC is 64.07, 125.78, and 115.85 CPU seconds, respectively. It is worth noting that the time required for data exchange between the controllers and the building system is significantly smaller than the computation time required to solve the optimization problems. Therefore, all three MPC controllers can be used online considering the 10-minute control interval.

##### 4.2. PCDL model verification

This section aims to evaluate the prediction and generalization performance of the PCDL model in building thermal modeling by comparing it with an LSTM model, which is the most popular and successful NN model for approximating sequential dynamic systems. The LSTM model is a two-layer model consistent with the proposed PCDL model. The training procedure of the PCDL and LSTM models is presented in Section A1 of the Appendix. The training loss profiles are presented in [Fig. A1](#) and [Table A1](#). [Fig. 5](#) presents the indoor temperature and relative humidity prediction results from January 1st to January 14th for thermal zone 1 by using the PCDL model and the LSTM model. Yellow lines represent the PCDL prediction results. Purple lines represent the LSTM prediction results. Grey lines are measurement data generated from the EnergyPlus model. Following the operation schedule, the indoor temperature is maintained at around 23°C, and the indoor relative humidity is maintained between 40 and 60% from 8:00 to 22:00. The models predict indoor conditions (6) hours in advance, using the latest measurement data as input. Both the PCDL and LSTM models present sufficient prediction accuracy in the training dataset.

Furthermore, [Fig. 6](#) displays the mean absolute error (MAE) of the predicted indoor temperature and relative humidity in each interval of the prediction horizon. Yellow lines and shaded areas represent the PCDL prediction MAE values. Blue lines and shaded areas represent the LSTM prediction MAE values. The shaded areas indicate the range between the quarter and three-quarter numbers of the MAE values. The results were computed based on the 6-hour predictions from January 1st to January 14th. The PCDL model has slightly higher MAE values than the LSTM model, which is mainly due to constraints on the weighting parameters and the specified PCDL model structure. The constraints reduce the prediction accuracy of the PCDL model, while the RNN-LSTM model structure used in the LSTM model has fewer parameters than the standard two-layer LSTM model. Despite this, the PCDL model still demonstrates sufficient prediction accuracy, as seen in [Figs. 5 and 6](#). The relative prediction error of the PCDL model is less than 5% based on the prediction results. In subsequent sections, we will show that the PCDL model overcomes overfitting problems and has better generalization abilities, even though its prediction accuracy on the training dataset is slightly reduced.

[Fig. 7](#) shows the thermal zone 1 prediction results of the PCDL and LSTM model under varying heating and humidifying power. The grey lines are the results generated from the EnergyPlus model. Yellow lines are the prediction results of the PCDL model. Purple lines are the prediction results of the LSTM model. The simulations and predictions were conducted from 6:00 to 24:00 on January 1st. The EnergyPlus model maintains indoor temperature and relative humidity within the ASHRAE indoor thermal comfort standard [67] of 21°C – 24°C and 35% – 45%, reflecting the goal of the proposed MPC systems to maintain indoor comfort. However, the LSTM model fails to capture the dynamics in changing heating and humidifying power, as its prediction results

remain relatively constant. The reason is that the training dataset, generated with constant temperature and humidity setpoints, only includes a limited amount of indoor temperature and humidity dynamics. Despite its accuracy on the training dataset, the black-box LSTM model struggles to understand the relationship between the heating power and the indoor temperature or between the humidifying and heating power and the indoor humidity. In contrast, the PCDL model demonstrates improved performance in capturing heating and humidifying dynamics in the indoor environment. When heating power increases, the EnergyPlus-simulated and PCDL-predicted temperatures increase similarly. When heating and humidifying power are modified, the EnergyPlus-simulated and PCDL-predicted relative humidity values also change in a similar fashion. The PCDL model's generalization ability is significantly better than that of the black-box LSTM model. With simple physics consistency definitions, the PCDL model performs competitively in approximating input-output responses. The proposed PCDL model's key advantage is that it does not require any information on the building structure, materials, construction, or other details, reducing the need for expert intervention. The PCDL model enables end-to-end modeling using remotely transmitted data, making it suitable for establishing thermal models in most residential and office buildings.

#### 4.3. Control performance and discussions

In this section, the proposed PCDL-based MPC controller is compared to three other controllers for indoor climate control of Carpenter Hall on January 15th. The controllers being compared are the On/Off controller, the SSM-based MPC controller, and the LSTM-based MPC controller. The On/Off controller is designed with a switch On/Off temperature of (20.28°C, 23.89°C) and a switch On/Off relative humidity of (30%, 60%) based on the ASHRAE indoor comfortable temperature and humidity standard [68]. The MPC controllers follow the definition in Section 3.1, with the prediction models being the SSM, LSTM, and PCDL models, respectively. The specific settings of the MPC controllers include the following:  $W_u = 0.02$ ;  $W_e = 1$ ;  $PMV_{LB} = -0.5$ ;  $PMV_{UB} = 0.5$ ;  $u_{LB}$  and  $u_{UB}$  are determined based on the rated power of devices. The unit for all the power values is kW.

The average power consumption of each thermal zone from 8:00 to 22:00 on January 15th by using various controllers (on-off, SSM-based MPC, LSTM-based MPC, and the proposed PCDL-based MPC) is presented in Fig. 8. The power consumption comprises heating, cooling, and humidifying. The results show that the PCDL-based MPC controller leads to lower energy consumption, 5.8%, 4.5%, and 8.9% compared to on-off, SSM-based, and LSTM-based controllers. Fig. 9 illustrates the corresponding statistical PMV distributions of each thermal zone using different controllers. The results demonstrate the superior performance of the PCDL-based MPC controller in meeting indoor comfort requirements in all five thermal zones compared to the other controllers. To further quantify the indoor thermal comfort performance, the proportion of time spent within the comfort range during the control process is computed. The analysis shows that the PCDL-based MPC controller outperforms the On/Off, SSM-based, and LSTM-based controllers by improving indoor thermal comfort by 55%, 59%, and 64%, respectively.

Moreover, Figs. 10, 11, 12, and 13 present the PMV level and energy consumption profiles from 8:00 to 22:00 on January 15th using the

on-off controller, SSM-based MPC controller, LSTM-based MPC controller, and PCDL-based MPC controller, respectively. The purple lines are the PMV control profiles. The red dash lines are the lower bounds for PMV values. The orange, blue, and green columns are the heating, cooling, and humidifying power consumption, respectively. Intuitively, to minimize energy consumption and indoor comfort violation concurrently, the PMV value should be maintained around  $-0.5$ . From the PMV control profiles, the PCDL-based MPC controller performs better than the other controllers. It should be noted that LSTM-based MPC has the weakest performance in controlling PMV, even worse than the on-off controller. In thermal zones 1, 2, and 4, the controlled PMV values are lower than the lower bound over 88.2%, 69.4%, and 34.1% portion of the time, respectively, with the lowest PMV even reaching an unacceptable level of  $-1.5$ . The poor performance of LSTM-based MPC is due to its weak generalization ability, as discussed in Section 4.2.

## 5. Conclusion

This article proposed a novel PCDL building thermal modeling method and explored its applications in the MPC framework to optimize building energy efficiency and maintain indoor comfort. The physics consistencies in building thermal dynamics were first defined following physics laws. A two-layer RNN-LSTM model structure is used to construct the PCDL model that enforces positive constraints on the weighting parameters of the RNN cell to ensure physics consistencies. Subsequently, the PCDL-based MPC was formulated utilizing the PCDL model as the prediction model. The cost function and constraints in the PCDL-based MPC were designed to optimize both energy efficiency and indoor comfort. The applicability of the proposed PCDL model and PCDL-based MPC framework was demonstrated through a case study of Carpenter Hall, a two-floor office building located in Cornell University campus. The results showed that the proposed PCDL model had superior generalization ability and interpretability compared to the conventional LSTM model. Moreover, in comparison to the On/Off, SSM-based MPC, and LSTM-based MPC controllers, the PCDL-based MPC framework reduced the building's energy consumption by 5.8%, 4.5%, and 8.9%, and improved indoor thermal comfort by 55%, 59%, and 64%, respectively. The above study results demonstrated the significance of incorporating physics consistency definitions into data-driven models and reinforced the superiority of the PCDL-based MPC controller.

## Declaration of Competing Interest

The authors declare that they have no known competing financial interests or personal relationships that could have appeared to influence the work reported in this paper.

## Data availability

Data will be made available on request.

## Acknowledgments

This work was partially supported by the National Science Foundation under Grant CBET-1643244.

## Appendix

The Appendix provides supplementary information regarding the proposed PCDL-based MPC framework. In Section A1, the training settings and algorithms for the PCDL and LSTM model are provided. Section A2 contains the formulation of the linear PMV model, while the SSM is presented in Section A3.

## A1. Training setting and algorithms for the PCDL and LSTM model

The specific training settings for the training process of the PCDL and the LSTM models are listed below: Learning rate is 103; optimization algorithm is Adam; loss function is MSE. The training process was performed using a GTX 1660 Ti GPU with the support of CUDA parallel computing. The dataset used was generated from the EnergyPlus model discussed in Section 4.1 and was split into 80% training data and 20% validation data. The offline training time for the PCDL and LSTM models are 166.13 and 52.55 s, respectively.

The loss values for the training and validation dataset of the LSTM and PCDL models are shown in Fig. A1. The solid blue lines represent the training loss. The dashed yellow lines represent the validation loss. The PCDL model utilizes a warm-up training method for parameter initialization, where physics consistency inputs were emphasized by setting all relevant weighting parameters to one and tuning other parameters from zero. The warm-up training period is followed by a formal training period with relaxed constraints on the physics-related parameters. It should be noted that the PCDL model requires more epochs before convergence, which largely results from the self-defined constraints on the weighting parameters. The final loss values of the LSTM and PCDL models are presented in Table A1. Although the LSTM model has lower loss values in both the training and validation datasets, the results from Section 4.2 indicate that the PCDL model has acceptable prediction accuracy and superior generalization ability compared to the LSTM model.

### A2. Linear PMV model generation.

PMV is a complex index to evaluate occupants' indoor comfort, and several factors are taken into consideration: clothing insulation, metabolic rate, air temperature, air velocity, air relative humidity, and mean radiant temperature [53,69]. Specifically, the PMV index is calculated as the following:

$$PMV = (ae^{-bMR} + c)Q_{diff} \quad (A1)$$

where  $MR$  is the metabolic rate;  $Q_{diff}$  is the difference between the internal heat production and loss;  $a$ ,  $b$ , and  $c$  are linear parameters. Based on previous works [43], a simplified linear model can be obtained with assumptions on clothing insulation and metabolic rate and measurements of the air velocity:

$$PMV = \hat{a}T + \hat{b}T_{mr} + \hat{c}RH + \hat{d} \quad (A2)$$

$\hat{a}$ ,  $\hat{b}$ ,  $\hat{c}$  and  $\hat{d}$  are linear parameters;  $T_{mr}$  is the mean radiant temperature, and is calculated by

$$T_{mr} = \left( T_{surf}^1 + T_{surf}^2 + \dots + T_{surf}^n \right) / (A^1 + A^2 + \dots + A^n) \quad (A3)$$

where  $T_{surf}^n$  and  $A^n$  are the temperature ( $^{\circ}$ C) and area ( $m^3$ ) of interior surfaces. Furthermore, the interior surface temperature and indoor temperature values are nearly identical in the EnergyPlus model used in this work. Therefore, we can apply the assumption  $T_{mr} = T$  and substitute it into Eq. (A2) as the following:

$$PMV = \hat{p}T + \hat{c}RH + \hat{d} \quad (A4)$$

where  $\hat{p} = \hat{a} + \hat{b}$ . Therefore, a linear PMV model is generated solely based on the indoor temperature and relative humidity.

### A3. State space model of building thermal dynamics.

The SSM of the building temperature dynamics is developed by using the BRCM toolbox [65]. BRCM applies the RC modeling method to generate bi-linear RC models based on building data, including geometry, construction, and material. Each element of the building system is approximated by a thermal RC node. The heating exchanges between the building and the exterior environment or HVAC system are defined by a specified exterior heating flux model. The mathematical representation of the SSM is as follows:

$$\mathbf{T}_{k+1} = \mathbf{AT}_k + \mathbf{Bu}_k + \mathbf{Bz}_k + \sum_{n_u} (\mathbf{B}_{xu,n_u} \mathbf{x}_k + \mathbf{B}_{zu,n_u} \mathbf{z}_k) \mathbf{u}_{k,n_u} \quad (A5)$$

where the state  $\mathbf{T}$  includes the temperature of all building elements (rooms, walls, floors, ceilings); input  $\mathbf{u}$  includes the heating and cooling power of HVAC systems; disturbance  $\mathbf{z}_k$  includes the environment temperature and solar irradiances;  $\mathbf{A}$ ,  $\mathbf{B}_x$ ,  $\mathbf{B}_z$ ,  $\mathbf{B}_{xu,n_u}$ ,  $\mathbf{B}_{zu,n_u}$  are matrices with appropriate dimensions;  $n_u$  is the index of control variables.

Furthermore, the indoor relative humidity can be computed based on indoor absolute humidity and temperature. The relationship can be written as the following:

$$RH_k = \frac{100H_kP}{0.611\rho P_{sat}(T_k)} \quad (A6)$$

where  $H$  is the absolute humidity ( $kg/m^3$ );  $\rho$  is the air density ( $kg/m^3$ );  $P$  is the indoor atmosphere pressure (kPa);  $P_{sat}(T_k)$  is the saturated atmosphere pressure (kPa) at the given indoor temperature. The absolute humidity mass balance equation can be written as the following:

$$V \frac{dH}{dt} = \dot{m}_{ig} + \dot{m}_{vent} + \dot{m}_{dehum} \quad (A7)$$

where  $V$  is the volume of the considered zone ( $m^3$ );  $\dot{m}_{ig}$ ,  $\dot{m}_{vent}$ ,  $\dot{m}_{dehum}$  represent internal moisture gain ( $kg/s$ ), moisture gain from ventilation system ( $kg/s$ ), moisture loss by space dehumidification ( $kg/s$ ), respectively. The internal moisture gain is comprised of humidity from human respiration and other sources. The ventilation system's humidifiers add moisture to the thermal zones, and the humidifying power can be expressed as follows:

$$U_{hum} = \left( \frac{\dot{m}_{add}}{Cap_{nom}} \right) \cdot U_{nom} + U_{fan} + U_{stby} \quad (A8)$$

where  $\dot{m}_{add}$  is the water addition rate ( $kg/s$ );  $Cap_{nom}$  is the humidifier nominal capacity ( $kg/s$ );  $U_{hum}$ ,  $U_{nom}$ ,  $U_{fan}$ ,  $U_{stby}$  represent the humidifying power, nominal humidifier power, nominal fan power, and standby power, respectively. Moreover, the water addition rate is computed by the following:

$$\dot{m}_{air} \cdot R_{in} + \dot{m}_{add} = \dot{m}_{vent} \quad (A9)$$

where  $\dot{m}_{air}$  is the airflow rate (kg/s);  $R_{in}$  is the inlet air humidity ratio (kg/kg), which is set to be equal to the environment air humidity ratio. Combining Eq. (A5) to (A9), the SSM of building thermal dynamics is derived as the following:

$$\mathbf{x}_{k+1} = F_{SSM}(\mathbf{x}_k, \mathbf{u}_k, \mathbf{z}_k) \quad (\text{A10})$$

The system state  $\mathbf{x}$  includes the temperature of all building elements and the indoor relative humidity; input  $\mathbf{u}$  includes the heating, cooling, and humidifying power; disturbance  $\mathbf{z}$  includes the environment temperature, environment humidity, and solar irradiances.

## References

- [1] International Energy Agency. Buildings: A source of enormous untapped efficiency potential. <https://www.iea.org/reports/buildings2022>.
- [2] Gonçalves D, Sheikhejad Y, Oliveira M, Martins N. One step forward toward smart city Utopia: smart building energy management based on adaptive surrogate modelling. *Energ Build* 2020;223:110146.
- [3] Mariano-Hernández D, Hernández-Callejo L, Zorita-Lamadrid A, Duque-Pérez O, García FS. A review of strategies for building energy management system: Model predictive control, demand side management, optimization, and fault detect & diagnosis. *Journal of Building Engineering* 2021;33:101692.
- [4] Verma A, Prakash S, Srivastava V, Kumar A, Mukhopadhyay SC. Sensing, controlling, and IoT infrastructure in smart building: A review. *IEEE Sens J* 2019;19:9036–46.
- [5] Dong B, Prakash V, Feng F, O'Neill Z. A review of smart building sensing system for better indoor environment control. *Energ Buildings* 2019;199:29–46.
- [6] Djennouri D, Laidi R, Djennouri Y, Balasingham I. Machine learning for smart building applications: Review and taxonomy. *ACM Computing Surveys (CSUR)* 2019;52:1–36.
- [7] Kramer R, Van Schijndel J, Schellen H. Simplified thermal and hygric building models: A literature review. *Frontiers of architectural research* 2012;1:318–25.
- [8] Li Z, Han Y, Xu P. Methods for benchmarking building energy consumption against its past or intended performance: An overview. *Appl Energy* 2014;124:325–34.
- [9] Privara S, Cigler J, Váňa Z, Oldewurtel F, Sagerschnig C, Záčeková E. Building modeling as a crucial part for building predictive control. *Energ Buildings* 2013;56:8–22.
- [10] Crawley DB, Lawrie LK, Winkelmann FC, Buhl WF, Huang YJ, Pedersen CO, et al. EnergyPlus: creating a new-generation building energy simulation program. *Energ Buildings* 2001;33:319–31.
- [11] Beckman WA, Broman L, Fiksel A, Klein SA, Lindberg E, Schuler M, et al. TRNSYS The most complete solar energy system modeling and simulation software. *Renew Energy* 1994;5:486–8.
- [12] Kalamees T. IDA ICE: the simulation tool for making the whole building energy and HAM analysis. *Annex 2004*;41:12–4.
- [13] Mattsson SE, Elmquist H, Otter M. Physical system modeling with Modelica. *Control Eng Pract* 1998;6:501–10.
- [14] Sun B, Yang C, Wang Y, Gui W, Craig I, Olivier L. A comprehensive hybrid first principles/machine learning modeling framework for complex industrial processes. *J Process Control* 2020;86:30–43.
- [15] Peng GC, Alber M, Buganza Tepole A, Cannon WR, De S, Dura-Bernal S, et al. Multiscale modeling meets machine learning: What can we learn? *Arch Comput Meth Eng* 2021;28:1017–37.
- [16] Wu K, Xiu D. Data-driven deep learning of partial differential equations in modal space. *J Comput Phys* 2020;408:109307.
- [17] Wang S, Chen H. A novel deep learning method for the classification of power quality disturbances using deep convolutional neural network. *Appl Energy* 2019;235:1126–40.
- [18] Zhang L, Wen J, Li Y, Chen J, Ye Y, Fu Y, et al. A review of machine learning in building load prediction. *Appl Energy* 2021;285:116452.
- [19] Harb H, Boyanov N, Hernandez L, Streblow R, Müller D. Development and validation of grey-box models for forecasting the thermal response of occupied buildings. *Energ Buildings* 2016;117:199–207.
- [20] Ascione F, Bianco N, De Stasio C, Mauro GM, Vanoli GP. Artificial neural networks to predict energy performance and retrofit scenarios for any member of a building category: A novel approach. *Energy* 2017;118:999–1017.
- [21] Jayathissa P, Luzzatto M, Schmidli J, Hofer J, Nagy Z, Schlueter A. Optimising building net energy demand with dynamic BIPV shading. *Appl Energy* 2017;202:726–35.
- [22] Yang S, Gao HO, You F. Model predictive control in phase-change-material-wallboard-enhanced building energy management considering electricity price dynamics. *Appl Energy* 2022;326:120023.
- [23] Shamsi MH, Ali U, Mangina E, O'Donnell J. Feature assessment frameworks to evaluate reduced-order grey-box building energy models. *Appl Energy* 2021;298:117174.
- [24] Shamsi MH, Ali U, O'Donnell J. A generalization approach for reduced order modelling of commercial buildings. *J Build Perform Simul* 2019;12:729–44.
- [25] Karpatne A, Atluri G, Faghmous JH, Steinbach M, Banerjee A, Ganguly A, et al. Theory-guided data science: A new paradigm for scientific discovery from data. *IEEE Trans Knowl Data Eng* 2017;29:2318–31.
- [26] Raissi M, Perdikaris P, Karniadakis GE. Physics-informed neural networks: A deep learning framework for solving forward and inverse problems involving nonlinear partial differential equations. *J Comput Phys* 2019;378:686–707.
- [27] Kharazmi E, Zhang Z, Karniadakis GE. hp-VPINNs: Variational physics-informed neural networks with domain decomposition. *Comput Methods Appl Mech Eng* 2021;374:113547.
- [28] Yang L, Meng X, Karniadakis GE. B-PINNs: Bayesian physics-informed neural networks for forward and inverse PDE problems with noisy data. *J Comput Phys* 2021;425:109913.
- [29] Büning F, Huber B, Schalbetter A, Aboudonia A, de Badyn MH, Heer P, et al. Physics-informed linear regression is a competitive approach compared to Machine Learning methods in building MPC. *arXiv preprint arXiv:211015911*. 2021.
- [30] Drgona J, Tuor AR, Chandan V, Vrabie DL. Physics-constrained deep learning of multi-zone building thermal dynamics. *Energ Buildings* 2021;243:110992.
- [31] Gokhale G, Claessens B, Develder C. Physics informed neural networks for control oriented thermal modeling of buildings. *Appl Energy* 2022;314:118852.
- [32] Di Natale L, Svetozarevic B, Heer P, Jones CN. Physically consistent neural networks for building thermal modeling: theory and analysis. *Appl Energy* 2022;325:119806.
- [33] Hannan MA, Faisal M, Ker PJ, Mun LH, Parvin K, Mahlia TMI, et al. A review of internet of energy based building energy management systems: Issues and recommendations. *IEEE Access* 2018;6:38997–9014.
- [34] Mason K, Grijalva S. A review of reinforcement learning for autonomous building energy management. *Comput Electr Eng* 2019;78:300–12.
- [35] Shaikh PH, Nor NBM, Nallagownden P, Elamvazuthi I, Ibrahim T. A review on optimized control systems for building energy and comfort management of smart sustainable buildings. *Renew Sustain Energy Rev* 2014;34:409–29.
- [36] Yu L, Qin S, Zhang M, Shen C, Jiang T, Guan X. A review of deep reinforcement learning for smart building energy management. *IEEE Internet Things J* 2021;8:12046–63.
- [37] Drgona J, Arroyo J, Figueira IC, Blum D, Arendt K, Kim D, et al. All you need to know about model predictive control for buildings. *Annu Rev Control* 2020;50:190–232.
- [38] Shang C, You F. A data-driven robust optimization approach to scenario-based stochastic model predictive control. *J Process Control* 2019;75:24–39.
- [39] Hu G, You F. Multi-Zone Building Control with Thermal Comfort Constraints under Disjunctive Uncertainty using Data-Driven Robust Model Predictive Control. *Adv Appl Energy* 2023;9:100124.
- [40] Park JY, Nagy Z. Comprehensive analysis of the relationship between thermal comfort and building control research-A data-driven literature review. *Renew Sustain Energy Rev* 2018;82:2664–79.
- [41] Li H, Wang S. Comparative assessment of alternative MPC strategies using real meteorological data and their enhancement for optimal utilization of flexibility-resources in buildings. *Energy* 2022;244:122693.
- [42] Hu G, You F. Renewable energy-powered semi-closed greenhouse for sustainable crop production using model predictive control and machine learning for energy management. *Renew Sustain Energy Rev* 2022;168:112790.
- [43] Yang S, Gao HO, You F. Model predictive control for Demand- and Market-Responsive building energy management by leveraging active latent heat storage. *Appl Energy* 2022;327:120054.
- [44] Chen W-H, Mattson NS, You F. Intelligent control and energy optimization in controlled environment agriculture via nonlinear model predictive control of semi-closed greenhouse. *Appl Energy* 2022;320:119334.
- [45] Hilliard T, Swan L, Qin Z. Experimental implementation of whole building MPC with zone based thermal comfort adjustments. *Build Environ* 2017;125:326–38.
- [46] Büning F, Huber B, Heer P, Aboudonia A, Lygeros J. Experimental demonstration of data predictive control for energy optimization and thermal comfort in buildings. *Energ Buildings* 2020;211:109792.
- [47] Büning F, Schalbetter A, Aboudonia A, de Badyn MH, Heer P, Lygeros J. Input convex neural networks for building MPC. *Learning for Dynamics and Control: PMLR*; 2021. p. 251–62.
- [48] Yang S, Wan MP, Chen W, Ng BF, Dubey S. Model predictive control with adaptive machine-learning-based model for building energy efficiency and comfort optimization. *Appl Energy* 2020;271:115147.
- [49] Baldi S, Korkas CD, Lv M, Kosmatopoulos EB. Automating occupant-building interaction via smart zoning of thermostatic loads: A switched self-tuning approach. *Appl Energy* 2018;231:1246–58.
- [50] Korkas CD, Baldi S, Kosmatopoulos EB. Grid-connected microgrids: Demand management via distributed control and human-in-the-loop optimization. In: *Advances in Renewable Energies and Power Technologies*; Elsevier; 2018. p. 315–44.
- [51] Nicodemus J, Kneifl J, Fehr J, Unger B. Physics-informed neural networks-based model predictive control for multi-link manipulators. *IFAC-PapersOnLine* 2022;55:331–6.
- [52] Alhajeri MS, Abdullah F, Wu Z, Christofides PD. Physics-informed machine learning modeling for predictive control using noisy data. *Chem Eng Res Des* 2022;186:34–49.
- [53] Fanger PO. Thermal comfort. Analysis and applications in environmental engineering. *Thermal comfort Analysis and applications in environmental engineering*. 1970.

- [56] Kerrigan EC, Maciejowski JM. Soft constraints and exact penalty functions in model predictive control. 2000.
- [57] Lu S, Lee JH, You F. Soft-constrained model predictive control based on data-driven distributionally robust optimization. *AIChE J* 2020;66:e16546.
- [58] Chen H, Allgöwer F. A quasi-infinite horizon nonlinear model predictive control scheme with guaranteed stability. *Automatica* 1998;34:1205–17.
- [59] Rawlings JB, Meadows ES, Muske KR. Nonlinear model predictive control: A tutorial and survey. *IFAC Proceedings Volumes* 1994;27:185–97.
- [60] Chen W, You F. Sustainable building climate control with renewable energy sources using nonlinear model predictive control. *Renew Sustain Energy Rev* 2022;168:112830.
- [61] Rao CV, Rawlings JB, Mayne DQ. Constrained state estimation for nonlinear discrete-time systems: Stability and moving horizon approximations. *IEEE Trans Autom Control* 2003;48:246–58.
- [62] Hespanha JP. Linear systems theory. Princeton University Press; 2018.
- [63] Goel S, Rosenberg M, Athalye R, Xie Y, Wang W, Hart R, et al. Enhancements to ASHRAE standard 90.1 prototype building models. Pacific Northwest National Lab. (PNNL), Richland, WA (United States); 2014.
- [64] Lawrie LK, Drury B, Crawley, Development of Global Typical Meteorological Years (TMYx). <http://climate.onebuilding.org2022>.
- [65] Sturzenegger D, Gyalistras D, Semeraro V, Morari M, Smith RS. BRCM Matlab toolbox: Model generation for model predictive building control. 2014 American Control Conference: IEEE; 2014. p. 1063–9.
- [66] Wetter M. Co-simulation of building energy and control systems with the Building Controls Virtual Test Bed. *J Build Perform Simul* 2011;4:185–203.
- [67] Ji W, Zhu Y, Cao B. Development of the predicted thermal sensation (PTS) model using the ASHRAE global thermal comfort database. *Energ Buildings* 2020;211:109780.
- [68] De Dear RJ, Brager GS. Thermal comfort in naturally ventilated buildings: revisions to ASHRAE Standard 55. *Energ Buildings* 2002;34:549–61.
- [69] Fanger P. Moderate thermal environments determination of the PMV and PPD indices and specification of the conditions for thermal comfort. ISO 1984;7730.